Microbial Range Expansions on Liquid Substrates

Severine Atis,[1,*] Bryan T. Weinstein,[2,†] Andrew W. Murray,[3,4] and David R. Nelson[1,2,3,4]

[1]*Department of Physics, Harvard University, Cambridge, Massachusetts 02138, USA*
[2]*School of Engineering and Applied Sciences, Harvard University, Cambridge, Massachusetts 02138, USA*
[3]*FAS Center for Systems Biology, Harvard University, Cambridge, Massachusetts 02138, USA*
[4]*Department of Molecular and Cellular Biology, Harvard University,*
Cambridge, Massachusetts 02138, USA

Despite the importance of fluid flow for transporting and organizing populations, few laboratory systems exist to systematically investigate the impact of advection on their spatial evolutionary dynamics. To address this problem, we study the morphology and genetic spatial structure of microbial colonies growing on the surface of a nutrient-laden fluid 10^4 to 10^5 times more viscous than water in Petri dishes; the extreme but finite viscosity inhibits undesired thermal convection and allows populations to effectively live at the air-liquid interface due to capillary forces. We discover that *S. cerevisiae* (baker's yeast) growing on a viscous liquid behave like "active matter": They metabolically generate fluid flows many times larger than their unperturbed colony expansion speed, and that flow, in turn, can dramatically impact their colony morphology and spatial population genetics. We show that yeast cells generate fluid flows by consuming surrounding nutrients and decreasing the local substrate density, leading to misaligned fluid pressure and density contours, which ultimately generates vorticity via a thresholdless baroclinic instability. Numerical simulations with experimentally measured parameters demonstrate that an intense vortex ring is produced below the colony's edge. As the viscosity of the substrate is lowered and the self-induced flow intensifies, we observe three distinct morphologies: At the highest viscosity, cell proliferation and movement produces compact circular colonies with, however, a stretched regime of exponential expansion; intermediate viscosities give rise to compact colonies with "fingers" that are usually monoclonal and then break into smaller cell clusters; at the lowest viscosity, the expanding colony fractures into many genetically diverse, mutually repelling, islandlike fragments that can colonize an entire 94-mm-diameter Petri dish within 36 hours. We propose a simple phenomenological model that predicts the early colony dynamics. Our results provide rich opportunities to study the interplay between fluid flow and spatial population genetics for future investigations.

Subject Areas: Biological Physics, Fluid Dynamics,
Soft Matter

I. INTRODUCTION

The transport of living organisms by fluid flows plays an important part in the natural world. Hydrodynamic transport shapes and reorganizes populations across all scales [1], mixing populations to uniformity or leading to the formation of spatial structures. For instance, turbulent mixing near the surface of oceans and lakes can cluster phytoplankton blooms into patchy, fractal-like spatial structures [2,3] that lead to ecological niches and genetic heterogeneity [4–6].

Microbial populations expanding into unoccupied territory on agar plates, or range expansions, have been used as a model system to investigate how population spatial structure impacts evolution [7]. Range expansions develop spatial structure because a thin layer of cells at the population front divide and generate genetically similar daughters who are not pushed very far away before they themselves divide. As a result of this linear population bottleneck at the frontier, the colony loses genetic diversity as the expansion progresses and quickly segregates into large monoclonal sectors that reveal the evolutionary history of the colony in a process often referred to as "genetic demixing" [7]. Simplified stepping stone models with radial inflation have been used to describe the evolutionary dynamics of this process [8]. Microbial range

*severine.atis@gmail.com
†btweinstein@gmail.com

expansions revealed how various evolutionary forces, including selection [9–11], mutualism [12], competitive exclusion [13,14], and irreversible mutation [15], impact the dynamics of spatially structured populations.

Microorganisms growing on agar plates cannot be advected because the underlying substrate is a solid, mimicking range expansions on land. Although investigated theoretically [16–19], few laboratory systems exist to systematically study the interplay between the transport by fluid flow and spatial population dynamics. In this paper, we introduce a novel experimental system to grow microbial range expansions on the *surface* of a nutrient-rich fluid 10^4 to 10^5 times more viscous than water. The extreme viscosity of the liquid substrate enables capillary forces to confine the cells over a macroscopic, quiescent air-liquid interface, and typical settling velocities of isolated cells that leave the surface are less than a cell width per day. This unique system allows us to investigate microbial population morphology and genetic segregation patterns on liquid interfaces.

To our surprise, even in the absence of externally imposed flows [20], our experiments reveal that colonies of the budding yeast *Saccharomyces cerevisiae* induces strong outwards fluid flows in the surrounding substrate many times larger than the colony's natural expansion velocity. Remarkably, these flows arise from *nonmotile* organisms, which do not possess, e.g., the flagellar-induced motility of bacteria [21–23]. In this paper, we show how the induced fluid flow impacts colony morphology and genetic segregation patterns as the viscosity of the underlying substrate varies and investigate the origin of the induced flow.

Section II summarizes our most important experimental observations about the morphology and spatial population genetics of expanding yeast colonies on liquid substrates and identifies three regimes: colonies behave as compact circular colonies, circular colonies with fingers, or many solidlike repelling yeast fragments as the substrate viscosity is varied from high to low. In Sec. III, we describe our measurements of fluid flows generated near the surface of growing colonies and identify two distinct regimes. The experiments in Sec. IV argue that the fluid flow is not generated by surface-tension gradients (Marangoni flows), but is instead it is triggered when yeast metabolism decreases the density of the surrounding fluid, generating buoyant fluid flows via a baroclinic instability due to the pressure and density contours crossing each other at an angle in the vicinity of the colony. Fluid-mechanics simulations calibrated to experiment in Sec. V provide further evidence that the buoyancy-driven baroclinic instability is the source of the fluid flow, as the simulations can quantitatively predict experimental results. Finally, in Sec. VI, we present a simple phenomenological model in the spirit of the lubrication approximation that combines colony growth, expansion, and thinning to predict the

critical magenta metabolically induced radial flow velocity at which colonies cease being circular. We compare the predictions from the model to a phase diagram of yeast colony morphology over time as a function of viscosity. The model displays a conventional Fisher population wave in the absence of flow but predicts exponential growth of the colony radius in the presence of a flow. When this radial flow is too strong, we find a "thinning catastrophe," such that the colony thickness tends to zero and breaks apart. Our work suggests many interesting avenues for future exploration discussed in Sec. VII.

II. RANGE EXPANSIONS ON LIQUID SUBSTRATES

To ensure a macroscopic quiescent liquid surface, we perform experiments with fluids 10^4–10^5 times more viscous than water. The viscosity of the fluid is controlled by adding 2-hydroxyethyl cellulose, a long chain polymer, to YPD [yeast extract, peptone, dextrose (glucose)] microbial growth medium; see the Appendix A for additional experimental details. Characteristic polymer concentrations used in our experiments and corresponding substrate viscosities are given in Table I. Although the fluid has shear-thinning properties for shear rates $\dot{\gamma} \gtrsim 10^{-1}$ s^{-1} [24], as we discuss in Appendix B, the flow's typical shear rate is of the order of $\dot{\gamma} = u/H \sim 10^{-6}$–$10^{-5}$ s^{-1}, where u is the characteristic surface flow velocity, and $H \sim 1$ cm is the substrate fluid height, such that non-Newtonian effects are negligible in our experiment. In contrast to plates filled with hard agar which form a gel substrate with a shear modulus, cellulose polymers do not form a three-dimensional mesh, allowing the growth medium to flow.

Our large substrate viscosity prevents thermal gradients in the environment from driving undesired convection; no substrate fluid motion is observed due to stray thermal gradients or other sources in the absence of a colony growing on the surface. After deposition on the substrate, droplets containing yeast cells spread uniformly, allowing a dilute concentration of cells to be held at the air-liquid interface by capillary forces. The cells rapidly aggregate due to attractive forces: capillary forces at the interface [25] for large distances, and van der Waals forces between the

TABLE I. Newtonian approximation to the liquid substrate's viscosity at a shear rate of $\dot{\gamma} \sim 10^{-4}$ s^{-1} (Appendix B) at various concentrations 24 h after mixing it with 2-hydroxyethyl cellulose.

Polymer % (w/v)	η (Pa s)
2.0	54 ± 8
2.2	86 ± 13
2.4	140 ± 20
2.6	300 ± 45
2.8	450 ± 70
3.0	600 ± 90
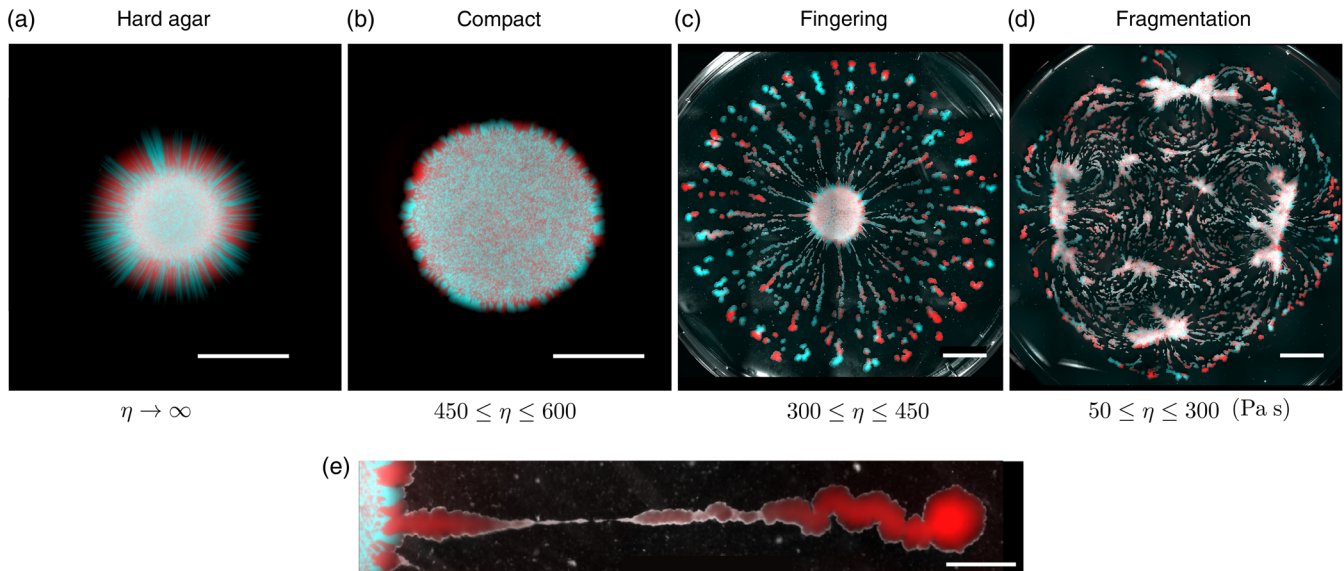
FIG. 1. Selected yeast colony morphologies on (a) a hard agar plate after 72 h of growth and on the surface of the viscous substrate with decreasing viscosities: (b) for $\eta = 600 \pm 90$ Pa s after 72 h of growth, (c) $\eta = 450 \pm 70$ Pa s after 84 h of growth, (d) $\eta = 300 \pm 45$ Pa s after 36 h of growth, and (e) magnification of a single representative finger from regime (c). Qualitatively similar morphologies are observed in the range of viscosities indicated in (b)–(d). The figure shows merged bright-field and fluorescent images White, transmitted bright field; red, YFP strains; cyan, mCherry strains. The scale bars in (a) and b) correspond to 5 mm, the scale bars in (c) and (d) to 10 mm, and to 2 mm in (e).

cells for short distances, in a process resembling spinodal decomposition or nucleation and growth [26]; see Fig. 12 and the Supplemental Material Video 0 [72]. Capillary forces are large enough to keep the cells on the surface of the fluid despite their slightly higher density than the media, allowing the colony to grow at the air-liquid interface over the typical several-day timescale of our experiments. The large substrate viscosity also leads to extremely slow sedimentation velocities of any small clumps of cells that break through the surface.

We follow the segregation of two selective neutral *S. cerevisiae* strains, genetically identical except for constitutively expressing different fluorescent proteins. The experiments are initiated by depositing cells in a 2-μL droplet of saturated overnight culture at the center of a 94-mm-diameter circular Petri dish filled with 40 mL of our viscous medium. The resulting colony expansion is then monitored over five days with a stereoscope (Appendix A). Shortly after cell growth and division begin, the microorganisms exhibit dramatically different growth dynamics relative to the well-studied hard agar plates and display a rich variety of morphologies depending on the media viscosity. We systematically vary the polymer concentration in the medium, allowing us to investigate the microbial population behavior over a range of dynamic viscosities η from 54 ± 8 to 600 ± 90 Pa s (corresponding from 2% to 3% w/v polymer; Table I). Figure 1 shows examples of yeast colonies after 72 hours of growth on a hard agar gel plate, compared to growth on liquid substrates for three different viscosities.

At the highest viscosity studied, $\eta = 600 \pm 90$ Pa s, the yeast cells form a single compact circular colony that expands radially over time (see Supplemental Material Video 1 [72]). However, unlike colonies on solid media where genetic drift dominates very close to the original frontier of the inoculation [7], colonies on the substrate have a stretched central region with genetic diversity (two colors are mixed together); demixing occurs only at a much larger colony radius, as displayed in Figs. 1(a) and 1(b) where the size of the initial inoculum is shown as a black dashed circle. Genetic domain walls with neutral strains impinge at right angles to a colony's front and are driven by interfacial undulations [7]. Yeast cells grown on the viscous liquid present much rougher colony fronts than on hard agar plates, leading to more irregular domain walls after the onset of genetic demixing. As the viscosity decreases to $\eta \approx 450$ Pa s, the initially circular colony forms numerous smaller microbial assemblies at its periphery on the media's surface. The front of the originally circular colony becomes unstable, and fingerlike structures form within the first 24 hours of growth. A large fingering colony spanning an entire Petri dish after 84 hours of growth can be seen in Fig. 1(c) and Supplemental Material Video 2 [72]; a high-magnification picture of a finger is shown in Fig. 1(e). These fingers form after demixing occurs, typically leading to monoclonal aggregates that grow and break up into small clusters, somewhat reminiscent of a Plateau-Rayleigh instability [27,28]. However, our system is complicated by active cell divisions and a colony-generated radial velocity field (see Sec. III). Below $\eta = 300 \pm 45$ Pa s, the initial

colony fractures into irregular pieces within the first 12 hours of expansion, behaving as if they have a shear modulus on our experimental timescales, and forms highly fragmented colonies as seen in Fig. 1(d) and Supplemental Material Video 3 [72]. Colonies in this regime break apart before genetic demixing occurs, resulting in genetically diverse growing fragments. The regularly interspersed fragments repel each other as they continue to grow, suggesting the existence of an underlying repelling flow. At the lowest studied viscosity $\eta = 54 \pm 8$ Pa s, these clusters of yeast cells propel themselves across an entire Petri dish within 36 hours, dispersing more than 1 order of magnitude faster than the same yeast strains growing on 2% hard agar plates (see Fig. 2 for the radial growth of our strains on agar and liquid substrates over time).

III. COLONY-GENERATED FLOW

In this section, we focus, for simplicity, on the high-viscosity regime $450 \lesssim \eta \lesssim 600$ Pa s, where yeast cells form a single approximately circular colony to investigate the coupling between its growth and the three-dimensional fluid flows generated in its vicinity. We image yeast
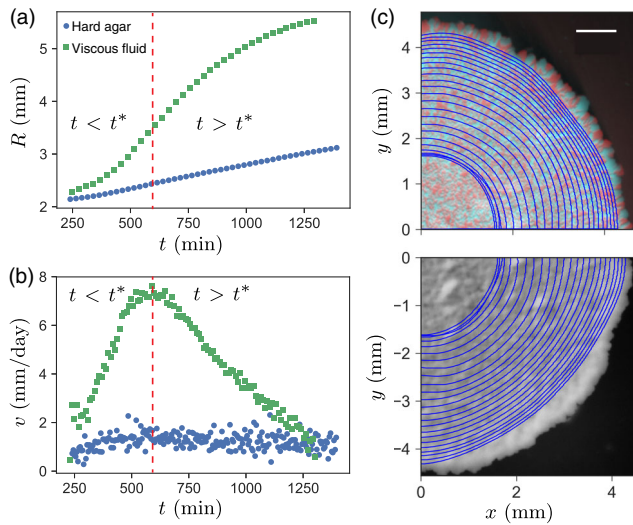
FIG. 2. (a) Azimuthally averaged yeast colony radius $R(t)$ during the first 24 h of growth on hard agar (blue circles) and on a liquid substrate with viscosity $\eta = 600 \pm 90$ Pa s (green squares). (b) The corresponding colony front velocity is extracted from $R(t)$. The colony exhibits two growth regimes on the liquid substrate: a superlinear regime for $t < t^*$ and a slowly decaying phase for $t > t^*$. We find that the colony front velocity approaches $v(t) = 0.5 \pm 0.05$ mm/day at long times ($t \gg t^*$) which is less than the velocity of yeast colonies growing on 2% hard agar plates. (c) Consecutive front spatial positions at equal 40-min intervals during the first 24 h of growth on liquid substrate with the same viscosity as (a) and (b), overlayed on top of a fluorescent (top) and a bright-field (bottom) image of the colony. Note that genetic demixing begins at the edge of the colony after the front slows down. The scale bar corresponds to 1 mm.

colonies growing during the first 48 hours after inoculation and in parallel extract the fluid velocity near the substrate's surface with particle image velocimetry (PIV). The fluid is seeded with a dilute concentration of $(10–20)$-μm fluorescent, neutrally buoyant polyethylene beads, and horizontal slices of the flow are followed at the desired height by varying the focal plane at which the beads' motion is tracked; see more details in Appendix A. Figure 2 displays the expanding colony average radius $R(t)$, velocity $v(t)$, and two-dimensional front profile over time extracted from bright-field images.

In contrast to yeast cells growing on hard agar plates which expand with approximately constant radial velocity [7,9,10,12], two distinct growth regimes with a crossover at a characteristic time $t^* \approx 600$ min can be identified on liquid substrates. At early times for $t < t^*$, the colony radius expands superlinearly with time and reaches a maximum horizontal growth velocity of $v \simeq 7.5 \pm 0.8$ mm/day, while for $t > t^*$ the expansion rate gradually slows down to $v \simeq 0.5 \pm 0.05$ mm/day over the rest of the experiment as shown in Fig. 2(b). This first, approximately exponential, growth regime when $t < t^*$ suggests that cells dividing throughout the entire colony contribute to its surface-area expansion, in contrast to growth on hard agar where only cells dividing near the front of the colony contribute to its expansion [7]. A comparison of the expansion rate of the colony with the spatial distribution of the strains reveals that genetically demixed sectors appear only after the front propagation slows down to $v \lesssim 2$ mm/day, as shown in Fig. 2(c), when only those regions exhibiting demixing at the edge of the colony are growing; see Supplemental Material Video 4 [72].

PIV measurements carried out in the same experiment near the surface of the fluid reveal an outward radial flow centered around the colony which begins soon after the first cell divisions occur; two-dimensional snapshots of the velocity field are displayed in Figs. 3(a)–3(c) for $t < t^*$, $t > t^*$, and $t \gg t^*$, respectively, while Figs. 3(d)–3(f) display the evolution of the azimuthal average of the velocity field $u_r(r, t) \equiv u(r, t)$ over time. The flow is radially symmetric, reflecting the circular colony shape at high viscosity, and its overall magnitude increases within 24 hours after inoculation (Supplemental Material Video 5 [72]). Two distinct regimes can be identified. At early times, for $t < t^*$, the radial velocity profile exhibits a maximum near the edge of the growing colony, whose value increases in time and peaks at $u = 6 \pm 0.8$ mm/day for $t \simeq 560$ min after inoculation and rapidly decreases away from the colony. The similar values and variation exhibited by the colony front propagation velocity $v(t)$ for $t < t^*$ and displayed in Fig. 2(b) suggest that the fluid is radially pushed outwards by the exponentially expanding colony during this time period.

However, as the expansion slows down after t^*, a secondary peak with a smaller amplitude can be observed
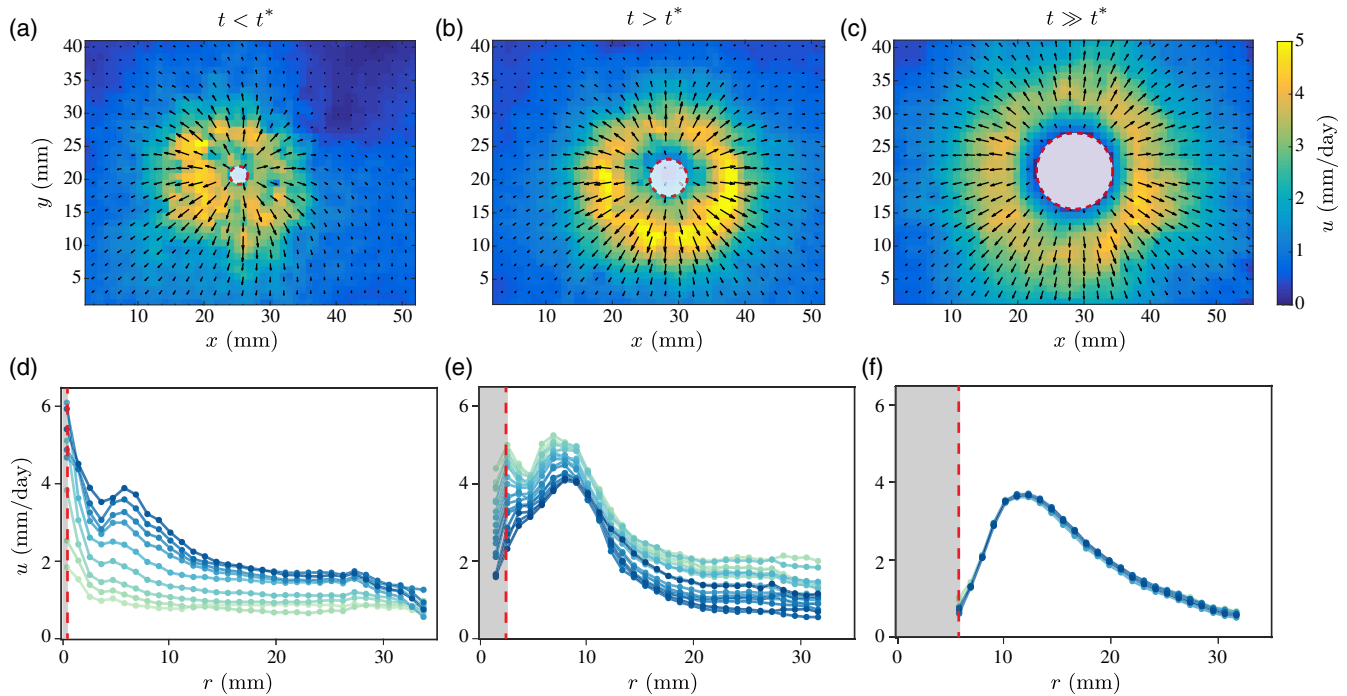
FIG. 3. Experimental flow field at the viscous substrate's surface over the first 48 h for compact yeast colony growth at a substrate viscosity of $\eta = 600 \pm 90$ Pa s for $t < t^*$ (a), $t > t^*$ (b), and $t \gg t^*$ (c). Each represented velocity field is averaged over 3 h. The central gray region delineated by red dashed lines indicates the growing colony's radius position masking the fluorescent beads; we cannot directly measure the velocity below the colony with this experimental setup. The color map represents the flow velocity amplitude. The azimuthal average of the velocity radial profile is plotted every 10 min for $t < t^*$ (d) and every 20 min for $t > t^*$ (e) and $t \gg t^*$ (f). The lines' intensity increases chronologically with times.

in Figs. 3(d) and 3(e). Within 48 hours, it approaches a time-independent velocity of $u = 4 \pm 0.5$ mm/day shown in Fig. 3(c) at about 1.5 colony radii away from the colony center despite the fact that the colony expansion velocity slows to $v(t) \lesssim 0.5 \pm 0.05$ mm/day (Supplemental Material Video 6 [72]). These observations suggest that the expanding edge of the colony pushing the surrounding fluid is not the unique origin of the observed flow, and another mechanism is generating the flow in the surrounding media for $t \gg t^*$, an idea we pursue in the next section.

IV. BAROCLINIC INSTABILITY

Plates filled with viscous media and monitored for 24 hours under conditions identical to our experiments show no evidence of flow in the absence of growing yeast cells, suggesting that the colony metabolism is responsible for the flow observed at $t > t^*$. A wide variety of microbial organisms exploit Marangoni flows [29] to facilitate their horizontal displacement across liquid interfaces by locally reducing the surface tension [30–32]. Yeast cells secrete a wide variety of molecules in their vicinity, including ethanol and pheromones, which could potentially lower the substrate surface tension in the colony surrounding. Surfactant-releasing particles, such as camphor boats, can lead to the formation of mutually repelling assemblies [33],

similar, for example, to the fragmented yeast aggregates we observe under the experimental conditions shown in Figs. 1(d) and 11. On the other hand, the yeast cell metabolism could also generate large enough gradients in the surrounding fluid's temperature or solute concentration to produce local differences in density and drive buoyant flows in the presence of a gravitational field [34]. However, as shown in the work of Benoit et al. [35], temperature gradients can be ruled out because heat diffuses over 200 times faster than small-molecule solutes (such as glucose) in water, minimizing resulting density gradients, and because the coefficient of thermal expansion is so much smaller than the coefficient of solute expansion; large temperature differences (several degrees Celsius) would be required to create the same density difference as a small change in solute concentration (see Appendix C for additional details).

In order to discriminate between these different sources of flow, we conduct a series of experiments where we anchor the colonies on a thin layer of agar to the top, bottom, and side of sealed chambers filled with our viscous media, as shown in Figs. 4(a) and 4(b). We find that colonies create fluid flows similar in magnitude to experiments when the air-liquid interface is present, regardless of their position in the chamber (even when placed at the top of the sealed chamber), and the induced fluid flows always
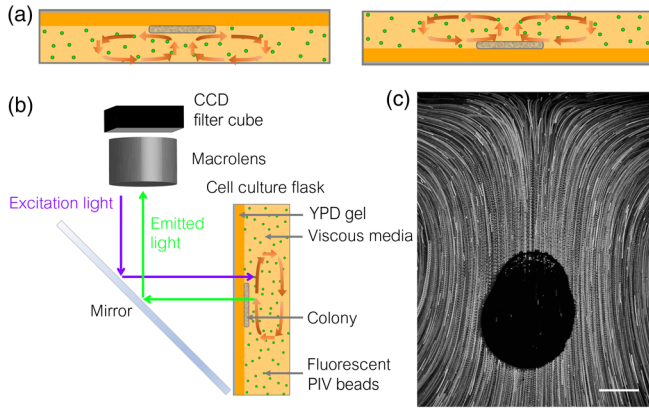
FIG. 4. Experimental setup for a yeast colony growing on a thin layer of agar in a sealed container filled with the viscous liquid; no liquid-air interfaces are present, removing the possibility of Marangoni flows. (a) The colony is anchored to the top or bottom walls of a Petri dish and (b) on the side wall of a culture flask. Gravity points downward, and the fluid is seeded with fluorescent PIV beads to track fluid motion. (c) Fluid flow streamlines near the yeast colony (the dark circular patch) in the same configuration as (b) during a time interval of $\Delta t \approx 6$ h obtained via maximum intensity projection. The scale bar corresponds to 5 mm.

oppose the direction of gravity. For instance, colonies entirely immersed in the liquid media and attached perpendicularly to the wall of the container create an upward flow over their surface; one large vortex on each side of the colony is partially visible in Fig. 4(c). Although these experiments do not rule out the possibility that surface-tension gradients generate flow when a free interface is present, they reveal that buoyant forces primarily drive the observed flows.

The flow thus systematically opposes the direction of gravity regardless of the position of the colony in the sealed chambers, suggesting that the cellular metabolism alters the density of the substrate by *depleting* nutrients in the surrounding fluid, for instance, by taking biomass from the solute to create progeny or by converting denser solute molecules into lighter ones (e.g., fermentation converts glucose to ethanol and carbon dioxide which are both less dense than glucose in water). In fact, similar behavior has been observed from *E. coli* growing in sealed chambers filled with liquid media [35]. Measuring the initial and final density of the medium after a yeast culture grows to saturation in YPD shows a decrease in density $\Delta \rho = -0.0090 \pm 0.0005$ g/mL, where the $\pm$ corresponds to the range of density differences we measure (see Appendix A for additional details), confirming that proliferating yeast cells reduce the density of the surrounding media.

However, in contrast to microbes growing at the bottom of a liquid-filled sealed container that can induce a classical Rayleigh-Taylor instability [35–37], where less-dense fluid

near the colony rises, the cells in our experiments grow on the surface of a liquid-air interface and cannot generate flow with this particular instability. Instead, the yeast produce a localized pocket of less-dense fluid *on top* of a more-dense fluid. In this configuration, the resulting density contours' misalignment with the hydrostatic pressure horizontal isobars leads to a thresholdless baroclinic instability. This type of instability, common in stratified fluids, generates vorticity and can be observed in atmospheric and oceanic flows [34,37,38].

The physical origin of the instability can be understood starting with the Navier-Stokes equations for the substrate fluid:

$$\frac{\partial \mathbf{u}}{\partial t} + (\mathbf{u} \cdot \boldsymbol{\nabla})\mathbf{u} = -\frac{1}{\rho}\boldsymbol{\nabla}p + \nu\nabla^2\mathbf{u} + \mathbf{g}, \quad (1)$$

where $\mathbf{u}$ is the fluid velocity, ρ the fluid density, p the pressure, $\nu = \eta/\rho$ the kinematic viscosity of the liquid medium, and $\mathbf{g} = -g\hat{\mathbf{z}}$ the gravitational force. Upon taking the curl of the fluid velocity $\boldsymbol{\omega} = \boldsymbol{\nabla} \times \mathbf{u}$, and neglecting vortex advection and stretching terms due to our low Reynolds numbers, we obtain for the vorticity

$$\frac{\partial \boldsymbol{\omega}}{\partial t} \approx \frac{1}{\rho^2}(\boldsymbol{\nabla}\rho \times \boldsymbol{\nabla}p) + \nu\nabla^2\boldsymbol{\omega}. \quad (2)$$

The viscous term $\nu\nabla^2\boldsymbol{\omega}$ simply redistributes the vorticity in the bulk fluid. However, the term $(1/\rho^2)(\boldsymbol{\nabla}\rho \times \boldsymbol{\nabla}p)$, often called the "baroclinicity" [38], generates vorticity whenever the contours of constant density ρ and pressure p cross at a finite angle. This is indeed the case in our experiments, as we discuss in the next section.

V. HYDRODYNAMIC SIMULATIONS

A. Origin of the baroclinic instability

To better understand how yeast colonies living at a liquid interface can trigger a baroclinic instability, we first assume a fluid at rest and numerically investigate how baroclinicity is created as the cells deplete the surrounding nutrient field by examining the resulting density and pressure contours. We assume the fluid has a density ρ which depends on the local concentration field $c(\mathbf{r}, t)$ of a diffusing nutrient solute such as glucose. The solute concentration is depleted near the metabolizing yeast cells such that the mass density of the fluid given by

$$\rho(\mathbf{r}, t) = \rho_0 + \delta\rho(\mathbf{r}, t) = \rho_0[1 + \beta c(\mathbf{r}, t)] \quad (3)$$

locally decreases, where ρ_0 is the fluid density without nutrient solute, $\beta = (1/\rho_0)[(\partial\rho)/(\partial c)]$ is the solute expansion coefficient, and $\delta\rho(\mathbf{r}, t) = \rho_0\beta c(\mathbf{r}, t)$ gives the local increase in density due to the presence of nutrients [35]. Let c_1 be the initial reference nutrient concentration before any metabolic depletion occurs, such that, close to the

metabolizing colony, there is a reduction in $\rho(\mathbf{r}, t)$ and $c(\mathbf{r}, t) < c_1$. In the absence of a flow, the momentum equation (1) simplifies to a hydrostatic pressure balance coupled to nutrient diffusion in the substrate fluid and becomes

$$-\boldsymbol{\nabla} p + \rho \mathbf{g} = 0, \qquad (4)$$

$$\frac{\partial c}{\partial t} = D\nabla^2 c, \qquad (5)$$

where D is the diffusion constant of the nutrient solute molecules.

We account for the colony nutrient absorption by imposing a nutrient mass flux normal to the colony's surface $\mathbf{j}_{\mathrm{col}} = ac\hat{\mathbf{n}}$, where a is the mass flux rate into the colony per unit nutrient concentration, and $\hat{\mathbf{n}}$ is the unit normal vector to the interface, such that larger nutrient concentrations lead to a larger nutrient absorption rate [39]. In contrast, no-nutrient-flux boundary conditions are applied elsewhere, on the walls of the domain away from the colony $D\boldsymbol{\nabla} c \cdot \hat{\mathbf{n}} = 0$. The mass flux due to transport and diffusion in the bulk fluid is given by $\mathbf{j}_{\mathrm{fluid}} = \rho_0 \beta (\mathbf{u}c - D\boldsymbol{\nabla} c)$. We assume that $\mathbf{u} = 0$ for now, and upon applying continuity on the solute flux across the colony boundary $(\mathbf{j}_{\mathrm{colony}} = \mathbf{j}_{\mathrm{fluid}})|_{\mathrm{colony}}$, the boundary condition can be rewritten as

$$(\boldsymbol{\nabla} c \cdot \hat{\mathbf{n}})|_{\mathrm{colony}} = \frac{c}{\ell}\bigg|_{\mathrm{colony}}, \qquad (6)$$

where $\ell = \rho_0 \beta D/a = 1.6 \pm 0.8$ mm acts as a characteristic nutrient-depletion length in the fluid that captures the interplay between nutrient diffusion and absorption by the bottom of the yeast colony. Here, ℓ is different from the nutrient screening length *inside* the yeast colony [39], as we discuss in Appendix D. Note that our yeast cells do not absorb the concentration field fast enough to warrant setting $c = 0$ at the interface between the colony and the fluid substrate as indicated by the dimensionless numbers that we discuss in Appendix E.

The actual colony expansion is neglected for simplicity, so we consider a colony of fixed radius R at the surface of the viscous fluid, in a radially symmetric Petri dish as shown in Fig. 5; the yeast colony is represented by the thick orange line. We use OPENFOAM 5.0 [40] to simulate Eqs. (4)–(6) using the program `diffusionPressureFoam` [41] and the measured parameters from Table II; additional details about the numerical scheme appear in Appendix F. Figure 5 displays the resulting density contours and isobars. Once the cells start absorbing nutrient mass from the fluid, a curved density gradient that conforms to the finite size of the colony is created in its vicinity, Fig. 16 shows an example of a corresponding simulated concentration field. The pressure contours, on the other
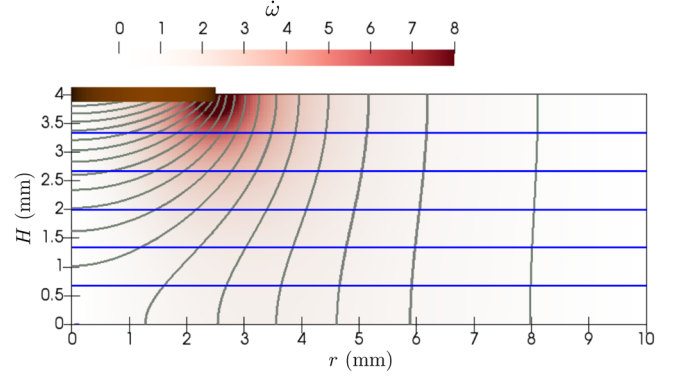
FIG. 5. Baroclinic vorticity generation rate $\partial \boldsymbol{\omega}/\partial t \approx (1/\rho^2)(\boldsymbol{\nabla}\rho \times \boldsymbol{\nabla} p)$ normal to a radial cross section before flow is initiated by a yeast colony fixed at the surface of the viscous fluid in a radially symmetric Petri dish. The colony position is indicated by the brown bar, the pressure isobars in blue, and the density contours in gray. The isobars are near horizontal due to small density differences originating from nutrient depletion (in this simulation, $\Delta\rho_{\mathrm{max}} \sim -0.003$ g/mL). Whenever the pressure and density contours cross at an angle, vorticity is generated via the baroclinic term in Eq. (2).

hand, remain nearly horizontal over the entire domain as the density differences due to solute depletion are so small. The finite crossing angle of the pressure and density contours leads to vorticity generation via the baroclinic term $(1/\rho^2)(\boldsymbol{\nabla}\rho \times \boldsymbol{\nabla} p)$ in Eq. (2) below the edge of the yeast colony, where the gradient of density is large and nearly perpendicular to the pressure gradient. As long as the yeast cells deplete the surrounding nutrients, the created density difference will generate vorticity via this thresholdless baroclinic instability.

B. Comparison with experiment

We now determine the flow produced by the baroclinic instability in the liquid substrate by simulating the hydrodynamic flow equations and compare our simulations with the experimental flow velocities. The diffusing solute field is coupled with the incompressible Navier-Stokes equations, and in the limit of small local density variations $\delta\rho(\mathbf{r})/\rho_0 \ll 1$, we can apply the Boussinesq approximation [34,35], such that Eq. (1) becomes

$$\frac{\partial \mathbf{u}}{\partial t} + (\mathbf{u} \cdot \boldsymbol{\nabla})\mathbf{u} = -\frac{1}{\rho_0}\boldsymbol{\nabla} p' + \nu\nabla^2\mathbf{u} + \beta c(\mathbf{r}, t)\mathbf{g}, \quad (7)$$

where the pressure $p' = p - \rho_0 gz$ is the pressure measured relative to the hydrostatic pressure at constant density ρ_0. We now introduce rescaled variables for space $\tilde{\mathbf{r}} = \mathbf{r}/H$, time $\tilde{t} = tD/H^2$, velocity $\tilde{\mathbf{u}} = \mathbf{u}H/D$, pressure $\tilde{p} = pH^2/D\eta$, and nutrient concentration relative to its value c_1 in the absence of the colony $\tilde{c} = c/c_1$, where H is the depth of the substrate fluid. In the creeping flow regime, appropriate to

TABLE II.   Model parameters and their experimentally measured values, where appropriate. For additional details, see Appendix D. Unless otherwise indicated, the error bars correspond to the standard deviation.

Parameter	Value	Units	Description
ν	100–1000	cm²/s	Kinematic viscosity; varies with polymer concentration
D	$2.4 \pm 0.2 \times 10^{-6}$	cm²/s	Diffusion coefficient of small nutrient molecules
ρ_1	1.015 ± 0.003	g/mL	Density of the viscous substrate with nutrients
βc_1	0.009 ± 0.0005	None	Product of the expansion coefficient β and c_1
ac_1	5 ± 1	pg/(μm²h)	Product of the mass flux into the yeast colony a and c_1
H	1–10	mm	Fluid height in the Petri dish ($H \approx 7$ mm for 40 mL)
r_{Petri}	43 ± 0.5	mm	Radius of the Petri dish
$\|\mathbf{g}\|$	9.81	m/s²	Gravitational acceleration
R	1–8	mm	Average radius of a yeast colony during an experiment
$\ell \equiv \rho_0 \beta D / a$	1.6 ± 0.8	mm	Characteristic nutrient-depletion length in the fluid.

our experiments, inertial terms on the left-hand side of Eq. (7) can be neglected, and the governing equations then become (see Appendix E for details)

$$\frac{\partial \tilde{c}}{\partial \tilde{t}} + \tilde{\mathbf{u}} \cdot \boldsymbol{\nabla}\tilde{c} = \nabla^2 \tilde{c}, \tag{8}$$

$$\nabla^2 \tilde{\mathbf{u}} - \boldsymbol{\nabla}\tilde{p} - \mathrm{Ra}\,\tilde{c}\,\hat{\mathbf{z}} = \mathbf{0}, \tag{9}$$

$$\boldsymbol{\nabla} \cdot \tilde{\mathbf{u}} = 0. \tag{10}$$

In Eq. (9), the Rayleigh number $\mathrm{Ra} = h^3 \beta c_1 g / D\nu$ compares the buoyant forces to the stabilizing effect of the viscous forces.

We can consider again a colony with fixed radius R, provided the characteristic eddy turnover time $\tau_{\mathrm{eddy}} \sim 1$ day for the baroclinic flow is much shorter than the characteristic radial colony growth time $\tau_{\mathrm{growth}} = R(t)/(dR/dt) \sim 10$ days for $t \gg t^*$. The colony expansion rate is slower than the induced flow velocity and starts behaving like a solid in this regime, so we apply a no-slip boundary condition just below the colony. We also apply a no-slip boundary condition to the walls of the Petri dish and a free-boundary condition to the air-substrate interface such that there is no normal velocity $v_z = 0$ and negligible shear stress $\partial v_r / \partial z = 0$. We apply the same nutrient-absorption boundary condition, from the previous section to the diffusing nutrient field below the yeast colony because the normal component of the fluid velocity at the boundary with the colony vanishes, and we also apply no-flux boundary conditions on both the Petri dish walls and fluid surface. We use OPENFOAM 5.0 [40] to solve the governing Eqs. (8)–(10) with the boundary conditions given by Eq. (6), using the program `stokesBuoyantSoluteFoam` [41] with the experimentally measured parameters in Table II; see Appendix F for additional numerical details.

The baroclinic effect leads to an intense vortex ring beneath the outer edge of the colony, as revealed by the transverse section shown in Fig. 6(a). The flow geometry

and intensity on the surface of the fluid resembles the experimental flow field shown in Fig. 3 around the colony. As shown in Fig. 6(b), the corresponding radial velocity profile at the fluid's interface is in good agreement with the experimental profile, with a strong peak at about 1.5 times the colony radius. Figure 6(c) compares the maximum radial velocity measured in the stationary flow regime reached after 48 hours in the experiments, with simulations
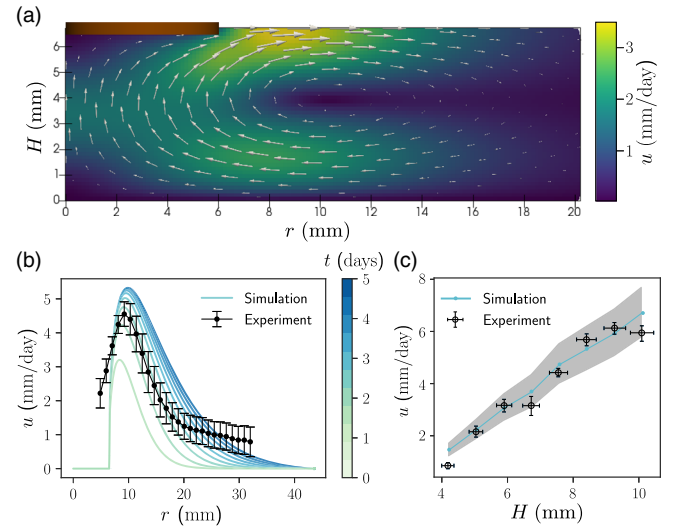
FIG. 6.   (a) Snapshot of the simulated flow field below the yeast colony (brown bar) after flow is initiated, for $t \gg t^*$. The simulated flow field qualitatively matches our experiments with a vortex ring produced around the colony. (b) Azimuthal average of the numerical flow field using the measured parameters in Table II plotted every 12 h at the substrate fluid surface. The black circles correspond to the experimental flow radial profile measured for similar flow parameters after 24 h of growth and an initial $\eta = 600 \pm 90$ Pa s. (c) Simulated and experimental peak radial velocity determined from PIV measurements 48 h after inoculation as a function of fluid height below the colony. The blue line with circles corresponds to the simulated values using the parameters in Table II, the black shaded region is the standard deviation of the simulated points, and the black circles correspond to experimental data.

as the substrate fluid height H is varied. Our minimal buoyant flow model tracks the experimental peak velocities, supporting the hypothesis of a buoyancy-driven flow produced by a baroclinic instability in our experiments.

VI. MODEL COUPLING GROWTH WITH DILATIONAL FLOW

In this section, we investigate how substrate viscosity influences colony morphology and describe a simple phenomenological model for colony growth, expansion,

and thinning in the spirit of the so-called lubrication approximation [42]. Figure 7 displays five characteristic colony morphologies over time growing on liquid media for the entire range of studied viscosities (Table I), from $\eta = 54 \pm 8$ Pa s to $\eta = 600 \pm 90$ Pa s. Our measurements of flow velocity shown in Fig. 3 reveal that metabolically driven buoyant flows become apparent as early as two hours after inoculation, suggesting that yeast cells can deplete enough mass to induce a flow even at this initial stage of growth. The first column to the left on Fig. 7 shows an enlargement of the colonies 12 hours after inoculation.
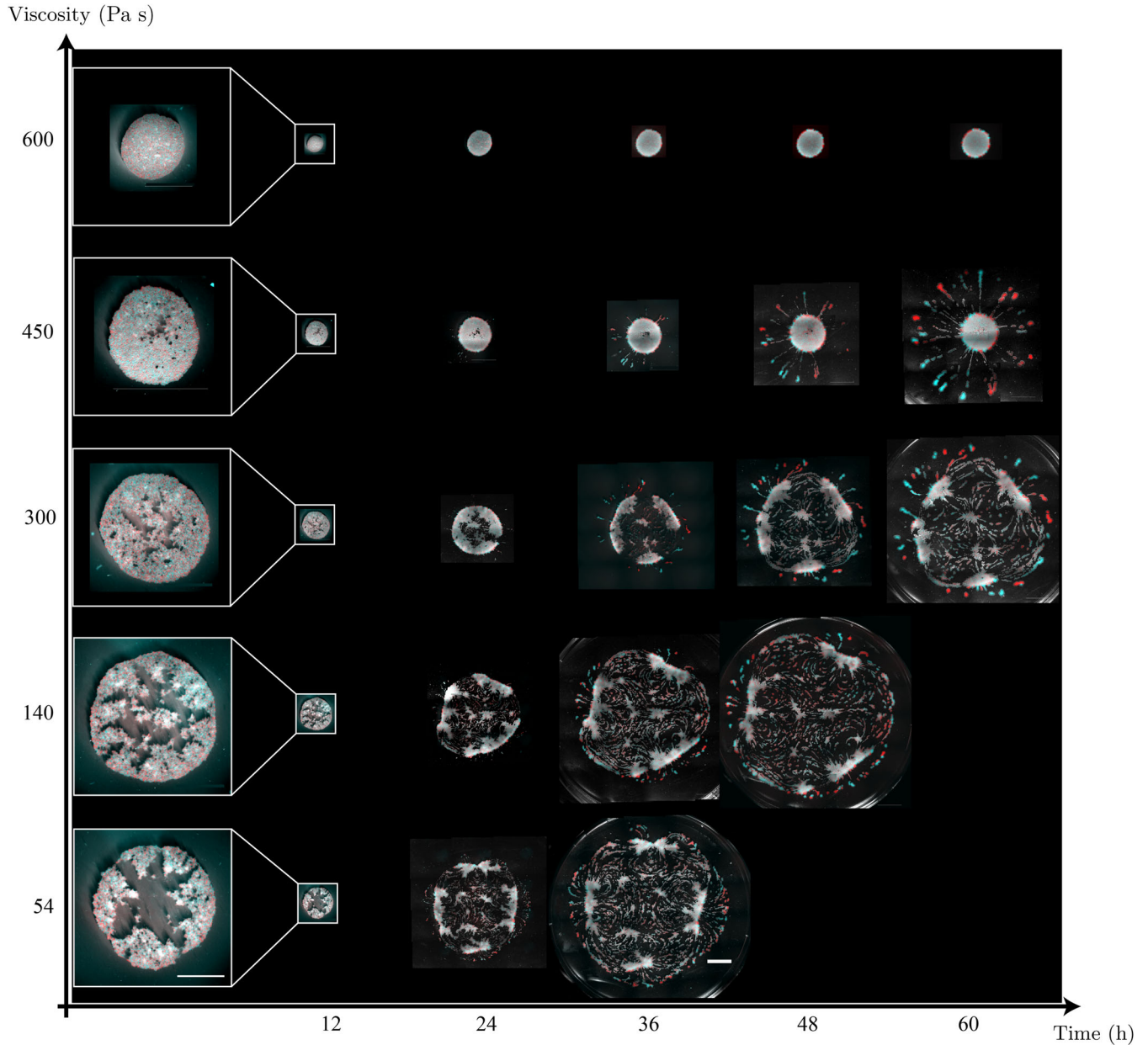
FIG. 7. Morphologies of yeast colonies growing on a liquid media substrate over time at a variety of viscosities. Quoted substrate viscosities are accurate to about 10% (see Table I). The figure shows merged bright-field and fluorescent images. White, transmitted bright field; red, YFP strains; cyan, mCherry strains. All images have the same scale, and the scale bar at the lower right corresponds to 10 mm. The left column is an enlargement of the colonies after 12 h of growth, and its scale bar corresponds to 5 mm.

Their shape already shows a strong dependence on the substrate viscosity, suggesting that the future morphology of the colony is determined during its early growth.

When viscosity decreases, the amplitude of the toroidal flow field beneath the colony increases and eventually applies enough force to alter the initial circular morphology of the colony. For instance, experiments performed at $\eta = 54 \pm 8$ Pa s indicate that the flow velocity can reach magnitudes up to 20 mm/day and apply non-negligible stresses on the colony. Once the cell division rate falls behind the colony's advancing front at $t \approx t^*$, the bulk of the colony ceases to behave as a liquid with internal motion due to cell division and begins to behave more like a visco-elastic material. Given the much faster fluid substrate velocities outside the colony relative to the colony expansion speed, the colony starts experiencing radial shear stresses imposed by the flow. One possible explanation for the especially intriguing colony morphology displaying multiple elongated fingers around the colony edge close to $\eta = 450 \pm 70$ Pa s could be a mechanism similar to viscous fingering instabilities. Under these conditions, competition between relaxation forces due to the attractive interaction between cells and an outward pulling force produced by the radial flow could drive an instability resembling those that arise in rotating oil films [43], suitably modified to allow for colony growth and the discreteness of the underlying cells. However, when the viscosity drops below $\eta \lesssim 300 \pm 45$ Pa s, the radial expansion imposed by the vortex ring under the colony starts to outcompete the colony expansion due to cell divisions, such that growth cannot accommodate the dilational flow during the initial stage. This results in a rapid separation of the cells, and holes start opening up within the center of the colony.

A complete understanding of the complex experimental behaviors described here (exponential stretching prior to genetic demixing, a fingering instability with fingers that break into dropletlike clusters and fragmentation; see Fig. 1) would require a detailed theory of the fluid dynamics of the substrate fluid coupled to the viscoelastic behavior of a colony of approximately 5-μm-sized cells with both excluded volume and attractive interactions, all while cells are actively dividing, as well as interacting with the substrate fluid during the range expansion. We hope that the results described here will encourage such theoretical investigations, which might also need to account for the discreteness of the cells in the colony and assess the impact of the fluid mechanics on the genetic demixing observed in our experiments.

Here, we propose instead a simple phenomenological model that provides insight into the exponential stretching and colony thinning during the early stages of the range expansion when the colony maintains its circular symmetry and behaves approximately like a two-dimensional liquid. In analogy with treatments of colony expansions on hard agar plates [44], we describe the dynamics of the colony height by a generalized Fisher population dynamics equation [45] for the colony height $h(\mathbf{r}, t)$, namely,

$$
\frac{\partial h(\mathbf{r}, t)}{\partial t} + \mathbf{\nabla} \cdot [h(\mathbf{r}, t)\mathbf{v}(\mathbf{r})]
$$
$$
= D_h \nabla^2 h(\mathbf{r}, t) + \mu h(\mathbf{r}, t)\left[1 - \frac{h(\mathbf{r}, t)}{h_0}\right], \quad (11)
$$

where $\mathbf{v}(\mathbf{r})$ is the advecting hydrodynamic flow velocity that acts on the colony, and μ is an effective colony vertical growth rate when its height is small. The quantity h_0 is the steady-state colony thickness in the absence of flow and spatial gradients of the height field, which we expect will depend on quantities such as nutrient penetration depth inside the colony [39] and strength of, e.g., the van der Waals and gravitational forces that attract the cells to the liquid substrate. The parameter D_h is a diffusion constant that promotes an approximately uniform colony height—a similar term appears in, e.g., the hydrodynamic equations that describe capillary wavelike excitations in thin helium films [46].

One source of the radially outward flows we observe near the surface during the early stages of our range expansions on liquid substrates is the outward pushing by the growing quasi-two-dimensional yeast colony. To determine the form of this contribution to the substrate flow, we assume that, at least during the early stages of the expansion, the colony behaves like a two-dimensional liquid where all the cells in the colony receive enough nutrients to actively divide. We further assume that the two-dimensional colony viscosity can be neglected compared to the overdamped frictional coupling to the liquid substrate. We can then apply a simple hydrodynamic model [47–50], which leads to

$$
\nabla^2 p_{2D} = -\gamma \mathbf{\nabla} \cdot \mathbf{v} = -\gamma \alpha_1, \quad (12)
$$

where p_{2D} is an effective two-dimensional pressure field inside the colony [50]. Here, α_1 arises from cell divisions that, as we show below, will give rise to a horizontal radial velocity field within the quasi-two-dimensional liquid colony averaged over the thickness of the colony. The quantity γ is a frictional coefficient due to the motion of the colony relative to the liquid substrate. If the liquid substrate has a dynamical viscosity η_s and depth H, in the limit of colony radius larger than H, we then expect $\gamma \approx \eta_s/hH$ [51], where h is the thickness of the colony. We can now exploit an electrostatic analogy, such that the two-dimensional pressure field inside the colony satisfies a Poisson equation and where the height-averaged growth rate α_1 determines a 2D "charge density." The colony velocity field (like the 2D electric field inside a charged disk in two dimensions) that solves Eq. (12) has the radially symmetric form:

$$\mathbf{v}(x,y) = \frac{1}{2}\alpha_1 r\hat{\mathbf{r}}, \qquad r = \sqrt{x^2 + y^2}. \qquad (13)$$

When coupled to an underlying viscous substrate fluid, this dilational flow field within the colony will act to induce flows in the underlying liquid, in qualitative agreement with our PIV measurements near the surface shown in Fig. 3(a). The development of expanding genetic patterns during the approximately exponential growth for $t < t^*$ is shown in Fig. 8(a). The figure highlights one particular feature inside the black dashed square which undergoes only a dilatation when expanding over time, as if the genetic patterns are painted on the surface of an inflating balloon, which is also consistent with Eq. (13). Estimates of this dilational expansion velocity for $t < t^*$ gives values of the order of 4–8 mm/day, the same order of magnitude as the colony front expansion velocity observed during the early exponential expansion regime.

The second source of the flow we need to account for is the more vigorous motion driven by the baroclinic instability. This flow is present for $t > t^*$ and becomes dominant at later growth stages for high substrate viscosity and at increasingly earlier times with decreasing substrate viscosity. Triggered by the metabolic uptake of nutrients, this additional flow is potentially responsible for the fingering and fragmentation instabilities observed when the substrate viscosity decreases and flow amplitude becomes larger. If we express the flow produced by cell divisions occurring throughout a circular colony in the form $\mathbf{v}_1(\mathbf{r}) = \frac{1}{2}\alpha_1 r\hat{\mathbf{r}}$, we expect then another contribution to this velocity of the form $\mathbf{v}_2(\mathbf{r}) = \frac{1}{2}\alpha_2 r\hat{\mathbf{r}}$ once the baroclinic instability establishes a vortex ring in the substrate fluid beneath the colony with a size of order 1.5 times the colony radius (Fig. 3). A simple model of a vortex ring submerged in substrate fluid with an image vortex ring with opposite circulation above the colony satisfies the requisite boundary conditions beneath the colony (the resulting velocity field resembles the magnetic field from a pair of anti-Helmholtz coils). This ansatz leads to a radial velocity field at the colony height which vanishes linearly in r for small r and falls off roughly like $1/r^4$ for r large compared to the colony radius. To check these ideas for the substrate-induced velocity field acting on the colony, we repeat the simulations of Sec. V B under identical conditions with, however, free instead of no-slip boundary conditions at the interface between the colony and the substrate fluid. We thus assume that active cell divisions throughout a circular colony cause it to behave like a two-dimensional liquid, with a contribution to the in-plane colony velocity field imposed directly by the substrate fluid. The resulting flow snapshot for the substrate fluid velocity field below the colony displayed in Fig. 8(b) is qualitatively similar to Fig. 6(a), indicating a submerged vortex ring. Now, however, the absence of a no-slip boundary condition leads to a velocity field right at the colony-substrate interface. The azimuthal average of our numerical flow field is shown in Fig. 8(c), again at 12-hour time intervals. The results are similar to Fig. 6(b), except that they clearly show a linear behavior of the velocity field underneath the colony, consistent with the ideas in the preceding paragraph.

With these motivations, it seems reasonable to assume that the advecting velocity field in Eq. (11) takes the form

$$\mathbf{v}(\mathbf{r}) = \frac{1}{2}\alpha r\hat{\mathbf{r}}, \qquad (14)$$

where α is an effective dilational flow parameter that includes the effect of the baroclinic instability as well as pushing generated by dividing cells within the colony. We expect α to increase with decreasing substrate viscosity, reflecting a stronger baroclinic instability.

With these assumptions, Eq. (11) takes the form

$$\frac{\partial h(\mathbf{r},t)}{\partial t} + \frac{1}{2}\alpha r\hat{\mathbf{r}} \cdot \nabla h(\mathbf{r},t)$$

$$= D_h \nabla^2 h(\mathbf{r},t) + (\mu - \alpha)h(\mathbf{r},t) - \frac{\mu h^2(\mathbf{r},t)}{h_0}. \qquad (15)$$

FIG. 8. (a) Magnification of experimental demixing patterns formed by two different yeast strains growing on a substrate with a viscosity $\eta = 600 \pm 90$ Pa s at different time points. The first three images have the same scale represented by the white bar on the upper right of the images; the scale bar corresponds to 100 μm. The final picture at the bottom shows the same feature at the larger colony scale; the scale bar now corresponds to 500 μm. (b) Snapshot of the simulated flow field below the yeast colony (brown bar) after flow is initiated. The simulated flow field is very similar to the one displayed in Fig. 6(a) except with a free boundary condition beneath the yeast colony. (c) Azimuthal average of the numerical flow field using the measured parameters in Table II plotted every 12 h at the substrate fluid surface with free boundary condition beneath the yeast colony.

In regions where the colony height is spatially uniform, we have for the height $h(t)$, $\{[\partial h(\mathbf{r}, t)]/(\partial t)\} = (\mu - \alpha)h(\mathbf{r}, t) - \mu h^2(\mathbf{r}, t)/h_0$, and thus,

$$h(t) = \frac{h(0)e^{(\mu-\alpha)t}}{1 + \frac{\mu h(0)/h_0}{\mu-\alpha}\left(e^{(\mu-\alpha)t} - 1\right)}. \tag{16}$$

We can now look for a radially symmetric solution with an interpolating steplike function $\Theta(x) = 1$, $x \ll 0$, $\Theta(x) = 0$, $x \gg 0$,

$$h(r, t) = h(t)\Theta[(R(t) - r)/\delta], \tag{17}$$

where $R(t)$ defines a colony radius smeared out over an interfacial width δ. It is easy to see from Eq. (15) that, provided $r \gg \delta$ and $r \gg \sqrt{D_h/\alpha}$, the colony radius grows exponentially in time:

$$R(t) = R(0)e^{\frac{1}{2}\alpha t}. \tag{18}$$

Figure 9 shows the numerical solution of Eq. (11), assuming radial symmetry for the colony height $h(\mathbf{r}, t) = h(r, t)$, at different values of α/μ using the program forcedThinFilmFoam [52]; see Appendix F for more details. In the absence of an advecting velocity field $\alpha = 0$ in Fig. 9(a), Eq. (15) has the usual Fisher wave solution of an outwardly expanding colony front circumference with constant velocity $v_F = 2\sqrt{D_h\mu}$ whenever the colony radius is much greater than the interfacial width $l_F = \sqrt{D_h/\mu}$ [45]. However, for nonzero α such that $\mu - \alpha > 0$ in Fig. 9(b), we find an *exponentially* fast advance of the wave: If the shoulder of the population wave in this case occurs at x_0 when $t = 0$, then the position of the shoulder at time t is at $x_0 \exp[(1/2)\alpha t]$, with a width δ of order $\sqrt{D_h/(\mu - \alpha)}$, consistent with our early-time observations in Fig. 2. In this regime, the colony advances but is thinned down to a height given by the long-time limit of Eq (16):

$$h^* = h_0\left(1 - \frac{\alpha}{\mu}\right). \tag{19}$$

Thus, with increasing α, the flow becomes stronger, and the exponential advance of the colony is faster but the colony becomes progressively thinner. Interestingly, when $\alpha = \mu$, Eq. (16) becomes $h(t) = h(0)/\{1 + [h(0)/h_0]\mu t\}$ and approaches zero as $h(t) \approx h_0/(\mu t)$ for large times. In fact, when time is substituted with R using Eq. (18), we find that at large times the height at the midpoint of the shoulder behaves according to

$$h_s[R(t)] \sim \frac{h_0}{\ln\left[\frac{R(t)}{R(0)}\right]}, \tag{20}$$
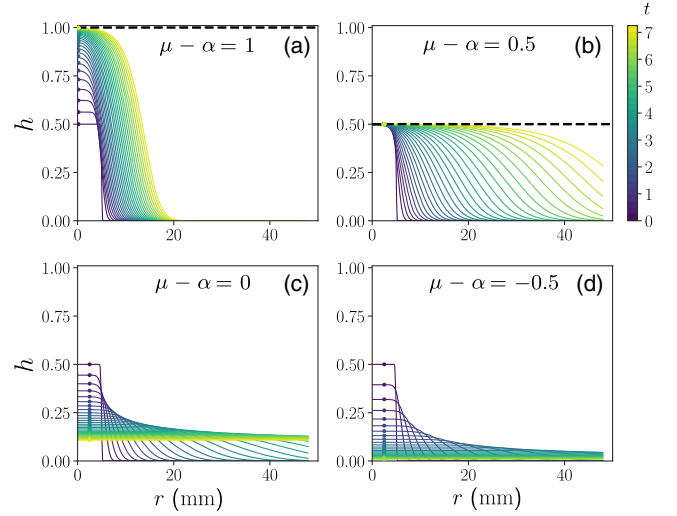
FIG. 9. Numerical solution of Eq. (11) for $h(\mathbf{r}, t)/h_0$ at different values of $\mu - \alpha$ and equal time intervals. The radial coordinate r is measured in units of $\sqrt{D_h/\mu}$, the width of the Fisher wave in the absence of a dilational flow. The colored dots correspond to the prediction of h as a function of time from Eq. (16) and show good agreement between the theoretical prediction and simulation. (a) For $\alpha = 0$, the colony height increases to $h/h_0 = 1$, and the front propagates radially with a constant velocity $v_F = 2\sqrt{D_h\mu}$ with $\mu = 1$. (b) When $\alpha < \mu$, the colony front propagation velocity increases exponentially with time, and the colony height decreases to $h^* = h_0(1 - \alpha/\mu) < h_0$. (c) When $\alpha = \mu$, the dilational flow is strong enough to decrease the colony height below one cell size and $h(t)$ goes to zero logarithmically with radius. (d) For $\alpha > \mu$, the colony thins exponentially fast, potentially signaling that holes open during its early exponential growth; these holes may be responsible for the highly fragmented colonies at later times.

such that h decreases logarithmically with the radius, leading to the formation of a wide plateau due to the extremely slow decay of h over time, as can be seen in Fig. 9(c). For sufficiently strong flows such that $\alpha > \mu$, there is a thinning catastrophe, as shown in Fig. 9(d), such that the colony population collapses at long times. In this limit, of course, the discrete nature of the cells making up the colony, neglected in Eqs. (11) and (15), becomes important.

Finally, we check the qualitative agreement between this simplified model and the experiments by determining the colony expansion rate during the superlinear growth regime $(t < t^*)$ as a function of substrate viscosity. A detailed measurement of the radial expansion coefficient's viscosity dependence $\alpha = \alpha(\eta)$ would provide a more quantitative test. Here, we explore this idea further by reproducing the same experiments as the ones described in Sec. II for two different substrate viscosities: By relating the above model predictions to the early colony morphologies, one may be able to estimate a critical viscosity below which the flow becomes strong enough to cause a thinning catastrophe.

As can be seen in the first column of Fig. 7, for $\eta \lesssim 300 \pm 45$ Pa s, holes start opening up in the center of the colonies during the early expansion, indicating that the flow dilation rate is larger than the colony height growth rate and corresponds to the height profile regime described by $\alpha > \mu$. Assuming $\eta \simeq 300 \pm 45$ Pa s is the highest viscosity at which we can observe a catastrophic thinning of the colony height in the early growth regime, our model suggests that $\alpha \approx \mu$ in this experiment.

Figure 10(a) displays the colony radius $R(t)$ over time growing on two different liquid substrates with viscosity $\eta = 600 \pm 90$ Pa s and $\eta = 300 \pm 45$ Pa s. The colony expansion rate described by Eq. (18) can then be estimated from an exponential fit of $R(t)$ for $t < t^*$ and gives $\alpha = 4.2 \pm 0.4$ day^{-1} for the higher viscosity and a larger rate $\alpha = 7.2 \pm 0.4$ day^{-1} for the lower viscosity. Assuming that the critical value of α, for which we have $\alpha \approx \mu$, is close to the colony expansion rate measured for $\eta = 300 \pm 45$ Pa s, we estimate $\mu \approx 7.2 \pm 0.5$ day^{-1}, which gives a characteristic division time of $\tau \approx 140$ min in the vertical direction of the colony, in approximate agreement with yeast colony growth rates on hard agar plates [50].

The dilational coefficient α in Eq. (14) is presumably a combination of the α_1 and α_2 contributions that we discuss above. Although it is difficult to determine the value of α_2 for $t < t^*$, as the metabolic velocity field is weaker at short times, we are able to isolate the constant α_1 related to the flow contribution coming from cell divisions at a liquid interface but *without* the enhanced dilational velocity due to the metabolic flow. To determine α_1, the same experiments are repeated on a much thinner 1-mm-thick layer of liquid substrate deposited on the top of a regular, nutrient-rich gel plate. This geometry allows us to damp out the baroclinic instability in the thin liquid layer and reveal a

nearly identical expansion rate this time, with $\alpha = 4.2 \pm 0.3$ day^{-1} for both $\eta = 300 \pm 45$ Pa s and $\eta = 600 \pm 90$ Pa s, suggesting that α_1 is independent of substrate viscosity for $300 \leq \eta \leq 600$ Pa s. Note that the measured value of α_1 is similar to the expansion rate α that we find for thicker substrates at higher viscosity, while it is significantly less than the measured α for the substrate with lower viscosity. This suggests that the metabolic flow does not contribute significantly to the colony expansion for $\eta = 600 \pm 90$ Pa s, while it considerably increases the colony dilation rate for $\eta = 300 \pm 45$ Pa s even at early times for $t < t^*$. Although further experiments would be required to fully map out the colony dynamics as a function of substrate thickness and viscosity, our experimental results suggest a qualitative agreement with Eqs. (11) and (15).

VII. DISCUSSION

We investigate the growth of yeast range expansions on the surface of an extremely viscous nutrient-rich liquid substrate. Capillary forces keep our yeast cells at the surface for many days, and the extreme viscosity of the fluid ensures that cell clumps that break the surface of the air-liquid interface settle slowly. The large viscosity also prevents thermal convection from mixing the media. Previous experiments of range expansions on solid agar media featured a thin layer of proliferating cells at the frontier of radially expanding circular colonies [7]. We find that colonies grown on a liquid medium, where the substrate can flow and friction between the cells and the medium is much lower, behave very differently.

In the early stages of these range expansions, for $t < t^*$, colony radii grow in a superlinear, approximately exponential fashion, and the growth is dominated by active cell divisions throughout the colony. However, for $t > t^*$, yeast metabolism generates fluid flows in the surrounding media many times larger than their basal expansion velocity. This flow dramatically alters the colony morphology, depending on the surrounding substrate viscosity.

Compact circular colonies grow for $\eta \approx 600 \pm 90$ Pa s (3.0% polymer), the largest viscosity we test, featuring a regime of roughly exponential stretching and thinning where strains remain mixed together and later a period of slow, linear expansion where strains genetically demix and resemble expansions on agar plates [7] with more wiggly domain walls. The expansion likely slows because of nutrient depletion.

As the viscosity of the medium decreases, hydrodynamic forces acting on the colony are eventually sufficient to produce fingering and fragmentation instabilities and lead to two additional morphologies. At intermediate viscosities between $\eta = 450 \pm 70$ Pa s and $\eta = 300 \pm 45$ Pa s (2.8%–2.6% polymer), compact colonies develop "fingers," a particular morphology that allows thin streams of cells to be ripped away from colonies resembling dendritic crystal growth in the presence of a solute-driven buoyant

(a) and (b) — plots of $R(t)$ (mm) versus t (min). Legend: 600 Pa s, 300 Pa s, Fit.
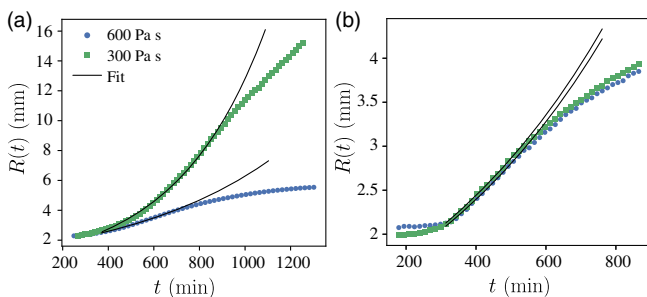
FIG. 10. (a) Colony radius as a function of time during the first day of growth for two different viscosities: blue circles, $\eta = 600 \pm 90$ Pa s; green squares, $\eta = 300 \pm 45$ Pa s; black line, exponential fit realized for $t < t^*$. The short-time behavior is consistent with an exponential growth of the colony radius in both cases, but the growth is much faster at lower viscosity. (b) Same as in (a) with experiments realized for colonies growing on a 1-mm-thin substrate liquid film on the top of a nutrient-rich gel layer. We find that the exponential fit realized for $t < t^*$ exhibits a similar expansion rate for both viscosities.

flow [53] or fingering instabilities in spinning drops [43] and Marangoni flow [54]. We attribute this liquidlike behavior at the colony perimeter to the lubricating effect of active cell divisions. The filaments then break into clusters via a process reminiscent of capillary forces in the Raleigh-Plateau instability [55,56] with, however, differences due to actively dividing discrete cells. The competition between the self-induced flow, diffusion of nutrients, and the attractive forces between the cells might trigger a selection for a characteristic finger width.

For viscosities lower than $\eta = 300 \pm 45$ Pa s, growing colonies exhibit solidlike behavior in the interior; they fracture into many irregularly shaped repelling islandlike fragments. These repelling fragments can colonize an entire Petri dish within 36 hours, presumably because each fragment metabolically generates its own submerged vortex ring. This conjecture about a vortex ring under each solidlike colony fragment is consistent with the image shown in Fig. 11, taken under experimental conditions similar to Fig. 1(d) but with a shallower substrate fluid. As opposed to the nearly monoclonal fingers separating from
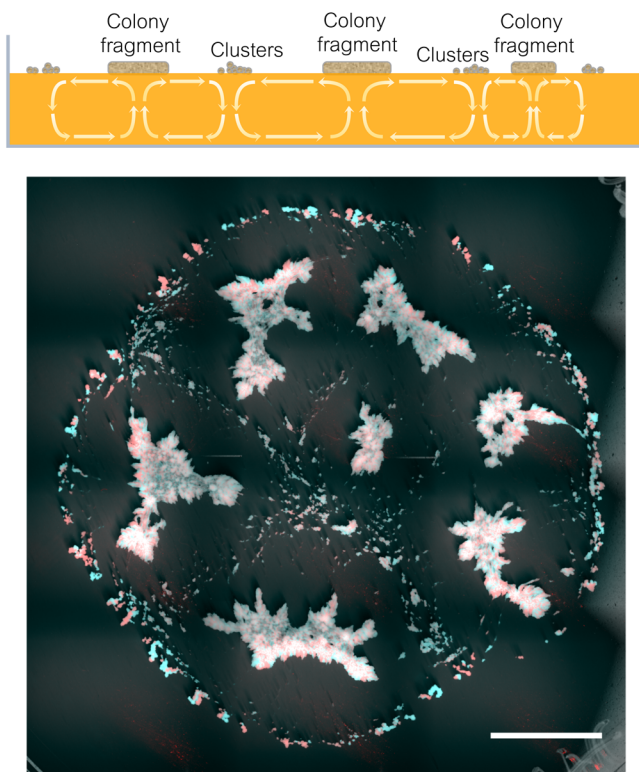
FIG. 11. Low-viscosity ($\eta = 300 \pm 45$ Pa s) range expansion on a liquid substrate in the fragmentation regime. This image is taken for $t \gg t^*$ in a single experiment under conditions similar to those in Fig. 1(d), except that the substrate fluid height is $H = 4$ mm instead of 7 mm. The more isolated cell fragments clearly collect on the midplanes separating the larger "continents," consistent with the downwellings associated with a vortex ring underneath each continent, as suggested by the sketch on the top. The scale bar corresponds to 10 mm.

the initial colony after demixing, islandlike fragments tend to be genetically diverse as the entire colony breaks apart.

Our experiments and simulations provide strong evidence that yeast metabolism generates fluid flow in the surrounding media via a baroclinic instability: Yeast colonies create a pocket of less-dense fluid *on top* of a more-dense one that generates vorticity near the colony edge when the isobars and isoclines of the underlying fluid cross each other at an angle. Minimal buoyant fluid-flow simulations calibrated to experiments with independently measured parameters capture our experimentally observed flow fields. Interestingly, as we discuss in Appendix D, these calibrations allow us to measure the mass flux rate into the yeast colony in rich-nutrient conditions as $ac_0 = 5 \pm 1$ pg/(μm^{2}h); the authors are unaware of other literature measuring this quantity. Furthermore, this mass flux rate is consistent with a nutrient screening length of about 50 μm inside yeast colonies (Appendix D), consistent with that measured in prior work [39].

Furthermore, colonies always generate fluid flows against the direction of gravity, regardless of their position in a sealed chamber, and we find that yeast cells grown to saturation in overnight culture decrease the surrounding media's density by $\Delta\rho = -0.0090 \pm 0.0005$ g/mL (Appendix A). We believe that surface-tension gradients (the Marangoni effect) plays only a minor role in generating the observed flows because yeast colonies attached to the surface of a sealed chamber generate a fluid flow comparable in magnitude and because the above arguments suggest that buoyancy alone sufficiently explains the phenomenon. To the best of our knowledge, this unusual baroclinic instability, while common in oceanic or atmospheric flows [34], has not been previously investigated in a biological context.

The work we describe here suggests a number of intriguing avenues for future work: For example, can other microorganisms growing on or near the surface of liquids generate buoyant flows similar to our experiments? Preliminary experiments with immotile *E. coli* colonies have exhibited similar flows when growing on the surface of liquid substrates with comparable viscosity and have also exhibited fascinating colony morphologies [20]. It is intriguing to speculate that similar instabilities might occur at much higher Reynolds numbers in the oceans, beneath plankton blooms confined to, say, the first 50 m of depth. It would also be interesting to experimentally test if microbial colonies that generate buoyant flows have a selective advantage relative to those that do not. Induced fluid flows clearly allow more efficient redistribution of nutrients and provide a mechanism for the more rapid dispersal of colony fragments. Preliminary numerical investigations when viscosity is lowered from infinity (i.e., modeling hard agar substrates), increasing the Rayleigh number from 0 to 10^4 in our Petri dish geometry, increases the nutrient-absorption rate of the yeast colony by a factor of about 1.5, suggesting

that colonies generating stronger buoyant flows could indeed have a selective advantage (see Appendix G for details).

Although yeast colonies might develop fluid-mechanics-like instabilities reminiscent of classical ones in the presence of flow [28,43,54,55], they differ in two key ways: (1) Dividing cells cause *growth* over time, stressing the need for further theoretical work to understand the instabilities arising from the competition between flow and growth, and (2) the discreteness of the dividing cells may play an important role near the thinning catastrophe that we discuss for a simple theoretical model in Sec. VI. The transition from an approximately exponential to a slower expansion rate, corresponding to the transition from liquid-like to solidlike behavior of the yeast colony, could also benefit from a fluid-mechanical perspective to model the yeast fingering instability, assuming a liquidlike behavior due to agitation by cell divisions at the frontier.

The origin of the *quantitative* differences between yeast colony growth on the highest-viscosity substrates and on hard agar plates such as the more wiggly genetic domain boundaries has yet to be understood. Systematic investigations of how colony morphology and genetic patterns vary with nutrient concentration (glucose) in addition to viscosity, similar to the pioneering work of Wakita *et al.* [44], would also be of interest. Furthermore, it is worth noting that we model the rheology of the liquid substrate as a Newtonian fluid despite the shear-thinning properties measured in the media at very large polymer concentrations as we discuss in Appendix B; future work should investigate how more pronounced non-Newtonian effects could impact the fluid flows induced by the yeast, in the context of microbial populations growing in mucus, for instance [57].

Lastly, the fluid that we use in this work is viscous enough that it can be advected at a velocity as low as 1 mm/day, matching the expansion rates of *E. coli* and the baker's yeast *S. cerevisiae* on agar [9,11] over an entire 9-cm Petri dish and several days of growth [20]. The extreme viscosity of the fluid allows for the imposition of slow controlled fluid flows at a macroscopic scale that can advect microbial colonies and provides an alternative to working with microfluidic devices where complications arise when microbes stick to the walls of their enclosure [58]. Using syringe pumps, one could impose well-defined flows on microbial colonies and systematically repeat previous experiments with microbial range expansions on hard agar plates [9–15] on viscous liquid substrates like those studied here but with additional types of advection. Investigating for instance the evolutionary dynamics of mutualistic strains that secrete public goods such as leucine and tryptophan [12] could be especially relevant because the secretions would be transported by the fluid flow. In conclusion, our results suggest that microbial range expansions on the surface of a highly viscous fluid

provide a versatile laboratory system to explore the interplay between advection and spatial population genetics.

APPENDIX A: MATERIALS AND METHODS

1. Liquid substrate preparation

To produce our highly viscous medium, standard rich-growth medium for yeast (YPD) consisting of 1% Bacto Yeast extract, 2% Bacto Peptone, and 2% anhydrous dextrose (glucose) is mixed in autoclaved water and filtered into a sterile glass bottle using a ZapCap (Maine Manufacturing item number 10443430) to remove contaminants. We then systematically increase the substrate viscosity by adding 2-hydroxyethyl cellulose, an extremely long-chain polymer with a viscosity-averaged molecular weight of 1.3×10^6 (Sigma-Aldrich product number 434981), at concentrations ranging from 2.0% to 3.0% w/v into 300-mL aliquots of the media, as shown in Table I. We use a strong magnetic mixer (IKA RCT basic magnetic stirrer) to rapidly stir the media with a sterile magnetic bar until it becomes homogenously viscous over the course of

three hours. We find that the model of the magnetic mixer is important; the mixer needs to be able to deliver enough torque to the stir bar so that it continues spinning as the media becomes very viscous. Furthermore, if we use too much media in the mixing flask (typically volumes greater than 300 mL), the polymer will not mix evenly. The final mixture is sterilized to avoid contaminants brought in from the polymer. Because the extreme viscosity of our fluid prevents it from being filtered, we sterilize it by microwaving it for three minutes (with a Panasonic model number NN-SN9735 microwave). In contrast to microwaving, sterilization via autoclaving produces inconsistent viscosities between replicates. We find that it is *essential* to let the media cool to room temperature in the bottle before pouring it into Petri dishes; yeast colony morphologies are not reproducible when inoculated onto substrates prepared with different heating protocols. As we discuss in Appendix B, the fluid's viscosity drops almost 20% over the first 24 hours and then slowly decreases as a function of time. The cells are consequently always inoculated 24 hours after pouring the media. Future work should investigate how to make the fluid viscosity more stable.

2. Strains

We use the prototrophic (capable of synthesizing all required amino acids) yeast strains yJHK041 and yJHK042 which are derived from the W303 background. The two strains are virtually identical and differ only by the expression of different fluorescent proteins under the control of an ACT1 promoter. yJHK041 expresses mCitrine and is colored red in our figures, while yJHK042 expresses mCherry and is colored cyan for visual clarity. yJHK041 has the genotype *MATa bud4 can1-100 prACT1-ymCitrine-tADH1-His3MX6:prACT1-ACT1*, and yJHK042 has the same genotype except with *ymCitrine* replaced with the *ymCherry*. The two strains have identical growth rates in liquid culture and expand at the same rate when deposited separately on agar plates.

3. Standard experimental setup

To prepare the saturated yeast cultures that we inoculate on our viscous media, we follow a similar procedure used for bacteria by Weinstein *et al.* [11]. We take a single colony of yeast growing on an agar plate and inoculate it in 10 mL of YPD media in a glass tube. The tube is then shaken overnight for roughly 16 hours at 30 °C as the yeast grows to saturation. The next morning, we use optical density measurements to place equal proportions of yJHK041 and yJHK042 in an Eppendorf tube with a final volume of 1 mL. After vortexing the Eppendorf tube, 2 μL of saturated culture is taken from the tube and inoculated on the surface of 40 mL of viscous fluid in a 94 × 16 mm Petri dish (Greiner Bio-One item number 633181), leading to an average fluid height of $H = 7 \pm 0.2$ mm. Throughout this paper, we use the same fluid height and volume unless
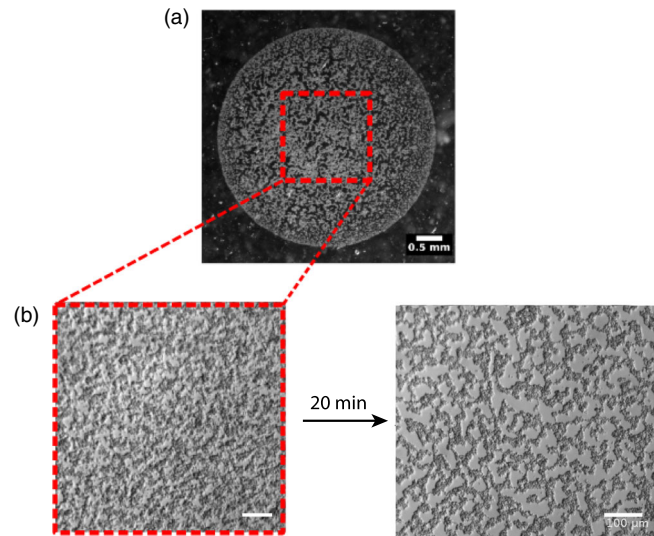
FIG. 12. Upon deposition on the highly viscous substrate fluid, yeast cells first spread uniformly in the circular inoculant region usually called the "homeland" [7] and then clump together via a coarsening process. (a) Distribution of cells 20 min after inoculation on the viscous substrate and (b) enlarged view immediately after inoculation (left) and after 20 min (right). The initially uniform distribution of yeast segregates into large clumps in a phase-separation process, suggestive of attractive interactions. The bottom scale bar corresponds to 100 μm.

specifically stated otherwise. Upon deposition, the cells immediately begin to aggregate and form clusters within 15 minutes as shown in Fig. 12. The plates are then wrapped with parafilm to inhibit drying and stored in a warm room held at 30 °C.

4. Imaging

The microbial colonies are imaged with an incubated Zeiss Lumar.V12 stereoscope held at 30 °C with both fluorescent (eYFP and mCherry) and bright-field channels. In order to image large fields of view (i.e., an entire Petri dish), we stitch many images together and blend their overlapping regions using AXIOVISION 4.8.2 software. Our fluid is viscous enough that panning the microscope stage does not adversely shake the fluid and microbes. Fluid flows are imaged by adding fluorescent green polyethylene microspheres between 10 and 20 μm in diameter (Cospheric item number UVPMS-BG-1.025 10–20 um–0.1 g) before mixing the media with the polymer. We then image the position of the beads every 5 to 15 minutes, depending on the mean flow rate, with the eGFP channel. By varying the focal plane at which we observe the beads, we can follow the flow in a horizontal slice at the desired height from the surface of the medium to the bottom of the Petri dish. The images are preprocessed and filtered before analyzing them with particle image velocimetry software (PIVLAB for MATLAB), and the resulting velocity fields are postprocessed using the MATLAB tool PIVMAT.

5. Density measurements

To test if yeast colonies deplete the density of the surrounding substrate as they metabolize, we compare the density of YPD media before and after the cells grow to saturation in it with an Anton Paar DMA 38 density meter. To conduct this experiment, we place a control test tube of YPD and another tube inoculated with our strains of yeast on a shaker overnight in a 30 °C room; the yeast culture grows to saturation. The next day, we centrifuge both tubes, depositing the yeast on the bottom of the second tube, and measure the supernatant density of each. We repeat this experiment three times and find that the average density of our control tube is $\rho_{\text{YPD}} = 1.0167 \pm 0.0003$ g/mL and that the density of the supernatant where the yeast grows is $\rho_{\text{saturated}} = 1.0077 \pm 0.0003$ g/mL, leading to a change in density of $\Delta\rho = -0.0090 \pm 0.0005$ g/mL where the $\pm$ corresponds to range of densities that we measure.

APPENDIX B: LIQUID SUBSTRATE RHEOLOGY

The substrate rheology is characterized with an Anton-Paar MCR 501 rheometer in a 50-mm disk geometry with a 1-mm gap. Figure 13(a) displays steady-state flow tests for various polymer concentrations realized with logarithmic sweeps of the shear rate ranging from 10^2 to 10^{-4} 1/s. Each point is averaged for several minute at 30 °C (the yeast incubation temperature), and the measurements are
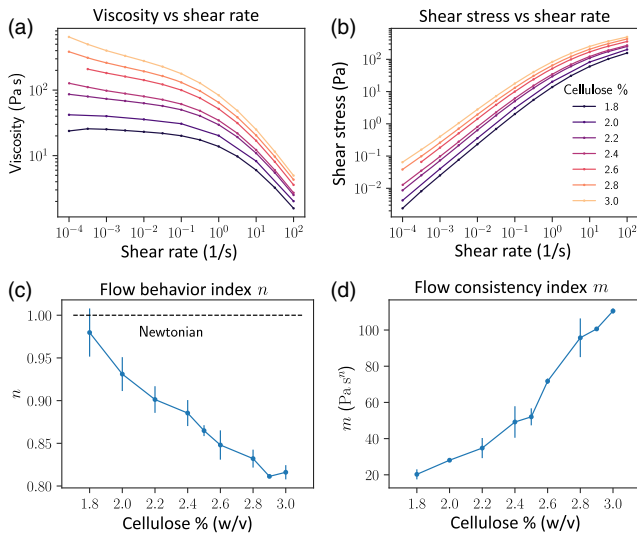
FIG. 13. (a) Shear viscosity and (b) corresponding shear stress for different polymer concentrations measured via steady-state flow tests. The fluid is weakly shear thinning for $\dot{\gamma} \lesssim 10^{-1}$ s^{-1} and reaches a Newtonian plateau at less than or equal to 2% polymer. For other concentrations, a power law of $\tau = m\dot{\gamma}^n$ describes the shear stress for shear rates of $\dot{\gamma} \lesssim 10^{-1}$ s^{-1}. (c) and (d) plot m and n as a function of polymer concentration; the fluid becomes more non-Newtonian (shear thinning) as more polymer is added.

performed a day after the viscous medium is microwaved, corresponding to the time that strains are inoculated on it.

Our viscous substrate exhibits a clear shear-thinning behavior; i.e., the viscosity decreases with increasing shear rate larger than $\dot{\gamma} \gtrsim 10^{-1}$ s^{-1} but presents a plateau for smaller shear rates. At cellulose concentrations higher than 2%, the viscosity continues to decrease with shear rate for $\dot{\gamma} \lesssim 10^{-1}$ 1/s, and we find an approximate power-law relation between the shear stress τ and shear rate $\dot{\gamma}$; Fig. 13(b) shows a fit to $\tau = m\dot{\gamma}^n$, in accord with the "power-law" model of Ostwald and de Waele [59–61], where the amplitude m is the flow consistency index, and the exponent n corresponds to the flow behavior index. The effective "Newtonian" viscosity of our fluid can then be expressed as $\eta(\dot{\gamma}) = m\dot{\gamma}^{n-1}$ [59], where $n = 1$ describes Newtonian fluids and $n < 1$ indicates shear-thinning behavior. We determine m and n as a function of polymer concentration by fitting the power-law behavior at shear rates lower than 10^{-1} 1/s as shown in Fig. 13. Our liquid substrate exhibits increasing shear-thinning behavior (decreasing n) with larger polymer concentration; we find $n = 0.93 \pm 0.05$ at 2% polymer and $n = 0.82 \pm 0.05$ at 3%, suggesting a small but measurable departure from Newtonian behavior across all polymer concentrations in this regime.

The typical shear rate in our experiments is on the order of $10^{-6} \leq \dot{\gamma} \leq 10^{-5}$ 1/s estimated from the measured surface flow velocity generated by the yeast colonies $1 \leq u \leq 20$ mm/day and with $\dot{\gamma} = u/H$ for a fluid with a typical height $H \approx 7$ mm. For simplicity, in this paper we describe our substrate as a Newtonian fluid and determine the viscosity from its value at a shear rate $\dot{\gamma} = 10^{-4}$ 1/s (the lowest shear rate at which the rheometer gives reproducible results); the corresponding values as we vary the polymer concentration are shown in Table I. The media rheology is monitored over one week and presents a slow decrease in viscosity as a function of time after being microwaved (less than 10% per day) and is neglected within the three-to-five-day timescale of our experiments. Although we did not investigated closely the rheology of hydroxyethyl cellulose polymer added in yeast complete synthetic media, the viscosity of these solutions appeared to be more stable as a function of time, and future work should consider using alternative yeast culture media.

APPENDIX C: ORIGIN OF THE BUOYANCY-DRIVEN FLOW

As we discuss in the main text, buoyant flows result from differences in density in the presence of a gravitational field [34], and, in our experiments, it could originate from gradients in fluid temperature and solute concentration. One possibility is that environmental temperature gradients (i.e., in the chamber where the yeast are imaged) drive fluid flows. As mentioned earlier, the very high viscosity of our

liquid media substrates coupled with estimates of critical Rayleigh numbers strongly suggest that stray thermal gradients would be insufficient to produce convection in our experiments [35]. In fact, plates filled with viscous media monitored over 24 hours show no evidence of a flow in the absence of yeast cells. The yeast colonies themselves must induce buoyant flows by generating local gradients in the surrounding fluid's temperature or solute concentration. Similar to the work of Benoit *et al.* [35], temperature gradients can be ruled out because heat diffusivity D_{heat} is much larger than the molecular diffusivity D_{glucose} of glucose in water, minimizing resulting density gradients caused by thermal gradients. The ratio of the heat diffusivity and molecular diffusivity is given by the Lewis number of our media: $L = D_{\text{heat}}/D_{\text{glucose}} \sim 300$ indicative of an isothermal fluid. In addition, the coefficient of thermal expansion is much smaller than the coefficient of solute expansion; large temperature differences (several degrees Celsius) would be required to create the same density difference from a small change in solute concentration [35]. Estimates of the yeast cell metabolic heat production seem insufficient to produce the requisite thermal gradient. For instance, comparing the density change induced only by the cells' glucose uptake $\Delta\rho_G$, with the density decrease due to the fluid thermal expansion caused by the heat produced during yeast glucose fermentation $\Delta\rho_T$, gives an estimate of $\Delta\rho_G/\Delta\rho_T \approx 1000$. This ratio suggests that the substrate density change is largely due to the glucose uptake rather than the metabolic heat produced by fermentation.

APPENDIX D: CALIBRATING SIMULATION TO EXPERIMENTS

Table II in the main text shows the values used to fit our model to experiment (i.e., Fig. 6), and the remainder of this appendix discusses how we obtain these values.

1. Viscous media density: ρ_0

As we discuss in Appendix A 5, we find that the density of YPD media *without* adding the cellulose polymer is $\rho_{\text{YPD}} = 1.0167 \pm 0.0003$ g/mL. Mixing hydroxyethyl cellulose with water within the range of the concentration we use in our experiments, i.e., between 2% and 3%, does not significantly affect the solution density [24]. Additional density measurements of the polymer solutions when mixed with YPD solutions [20] also do not show a significant change in density of the substrate within experimental error.

2. Solute expansion coefficient: β

The solute expansion coefficient β enters only in our dimensionless simulations via the combination βc_1 in the Rayleigh number,

$$\text{Ra} = \frac{h^3 \beta c_1 g}{D\nu},$$

where c_1 is the initial concentration of solute in the system. In our experiments, c_1 is also the *maximum* concentration, since uptake of nutrients and excretion of less-dense waste products leads to a net depletion of the effective concentration field. Hence, to estimate βc_1, we simply note that the density change when all solute is depleted is $\Delta\rho = -0.0090 \pm 0.0005$ g/mL from our experiments measuring the density of yeast overnight culture (Appendix A 5). Because the density of our media is $\rho = \rho_0(1 + \beta c)$, and after a day of growth in well-mixed culture, the glucose is completely depleted as the yeast can no longer reproduce, we estimate $\Delta\rho \approx -\rho_0 \beta c_1$, implying that $\beta c_1 = -\Delta\rho/\rho_0$. After including appropriate sources of error, we thus find $\beta c_1 = 0.009 \pm 0.0005$.

3. Diffusion constant: D

Yeast colonies deplete the density of the surrounding media in order to create more biomass. In the model used by Benoit *et al.* [35], cells can absorb molecules with a variety of sizes and with correspondingly different concentration fields and diffusion constants. Here, the change in density we observe in overnight culture $\Delta\rho = -0.009 \pm 0.0005$ g/mL is consistent with approximately all of the glucose (originally 2%) in the media being depleted within a factor of 2 [62]. For simplicity, we consequently use a single concentration field c to model the diffusion and absorption of glucose only.

The glucose concentration field in our liquid substrate is difficult to track. In order to estimate the diffusion constant in our medium, we instead track the diffusion of fluorescein molecules as a proxy for glucose in our substrate over the course of several days (see Ref. [20] for additional details). A circular droplet of approximately 7 mm in diameter is deposited on the surface of a thin 2.5-mm-thick layer of our viscous media. We use the Zeiss Lumar stereoscope to confirm that the concentration of fluorescein is proportional to its fluorescent intensity at a fixed exposure time by creating a dilution series. We then image the droplet and extract its radially symmetric concentration profile and repeat the process several hours later. The fluid is held at the same temperature as our colony expansion experiments (30 °C). The radial density profile of a diffusing concentration $c(\vec{r}, t)$ can be related to its original profile $c_{t_0} = c(r, t = 0)$ via an integral representation that depends on the diffusion constant D [63]:

$$c(r, t) = \frac{1}{2Dt} \int_0^\infty ds\, s\, c_{t_0} I_0\left(\frac{rs}{2Dt}\right) e^{-[(r^2 + s^2)/(4Dt)]}, \quad \text{(D1)}$$

where I_0 is the modified Bessel function of the first kind, and we take the limit of the plate radius to infinity for simplicity. We ignore diffusion in the third dimension (towards the bottom of the plate) as the fluid layer is small relative to the droplet diameter. We fit the fluorescein
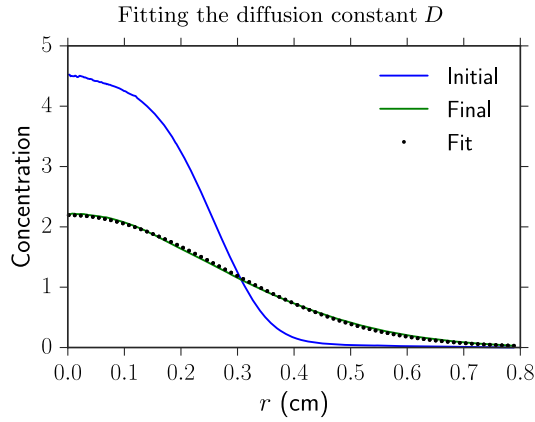
FIG. 14. Fit to the fluorescein diffusion constant D in our viscous fluid. The blue line corresponds to the measured initial radial profile, and the green line is measured the final profile. Black dotted line represents the profile predicted by Eq. (D1) with the best-fit value of D

FIG. 15. Simulated average flow velocity as a function of mass flux rate $j_{\text{colony}} = ac_1$ into a submerged yeast colony in rich nutrient conditions. The velocity field is determined above the center of the colony in the rising plume of fluid from the bottom to the top of the domain.

diffusion constant D in Eq. (D1) by inserting our experimentally measured initial concentration field at $c(r, t = 0)$, numerically evaluating the integral, and comparing the predicted concentration field at later times to our experimental measurements. We adjust the value of D using a least-squares fit to find the best fit to our experimental measurement.

Figure 14 displays the original radial profile of the fluorescein, the final profile, and the predicted fit from Eq. (D1) with the best value of D. We repeat this experiment three times on media with 2.0% and 3.0% polymer concentration and find identical diffusion constants within experimental error, $D = 2.4 \pm 0.2 \times 10^{-6}$ cm²/s. These results are consistent with the assumption that fluorescein diffusion is dominated by motion through the gaps between the long chains of hydroxyethyl cellulose polymer. Noting that the diffusion constants of fluorescein and dextrose (glucose) are similar in water at 25 °C: $D_{\text{fluorescein}} = 4.25 \pm 0.01 \times 10^{-6}$ cm²/s and $D_{\text{dextrose}} = 5.7 \pm 0.01 \times 10^{-6}$ cm²/s [64]. For simplicity, we use the measured diffusion constant of fluorescein in our simulations of the substrate fluid given by $D = 2.4 \pm 0.2 \times 10^{-6}$ cm²/s.

4. Mass flux rate into the yeast colony in rich-nutrient conditions: ac_1

We fit ac_1, the mass flux rate into the yeast colony in rich-nutrient conditions by calibrating our simulation to experiments in a situation which negates the effect of surface tension: A yeast colony anchored on a thin agar sheet on the bottom of a *sealed* Petri dish filled with our viscous nutrient-containing fluid at $\eta = 54 \pm 8$ Pa s [see Fig. 4(a) left]. Under these conditions, the simulated yeast colony nutrient uptake creates a buoyant plume in the direction opposing gravity, and the fluid flow reaches a maximum stable magnitude after about a day of growth.
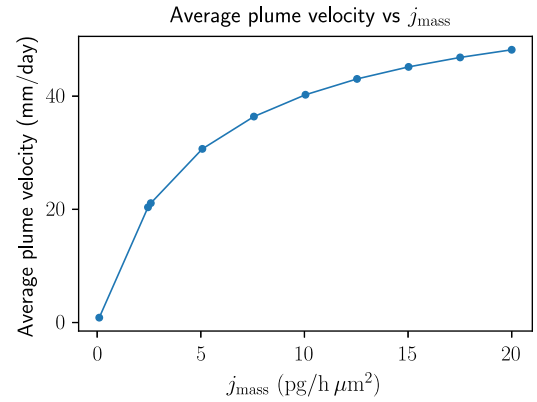
Note from the right side of Fig. 4(a) that the induced flow in this case *opposes* the outward-growth-induced expansion velocity of the colony. We adjust the product ac_1 until the simulated average flow velocity in the plume above the colony, as shown in Fig. 15, matches the average experimental velocity of tracer beads moving in the rising fluid from the bottom to the top of the container above the colony. The best match for $v_{\text{experimental}} = 30 \pm 10$ mm/day results in a value of $ac_1 = 5 \pm 1$ pg/(μm²h), where the error limits represent the standard deviation.

We now argue that this mass flux rate is consistent with a simple order-of-magnitude estimate and also show that it predicts a nutrient screening length inside yeast colonies in agreement with earlier investigations [39].

a. Order-of-magnitude estimate for ac_1

A single yeast cell consumes about $N \sim 10^{12}$ glucose molecules per cell division when fermenting at high glucose concentrations [65], and glucose has a molar mass of $M = 180.156$ g/mol. Yeast divide roughly every $\tau_g \approx 90$ min in rich media, have a radius of approximately $r_{\text{yeast}} \approx 2.5$ μm, and are approximately spherical when not actively dividing; they consequently have an area of $A_{\text{yeast}} = 4\pi r_{\text{yeast}}^2$. Therefore, the glucose mass flux into a spherical yeast cell must be on the order of

$$j_{\text{cell}} = a_{\text{yeast}}c \sim \frac{MN}{A_{\text{yeast}}\tau_g} \sim 2.5 \ \frac{\text{pg}}{\mu\text{m}^2\text{h}}. \quad \text{(D2)}$$

In nutrient-rich conditions, we assume that the concentration field is at its maximum value of $c = c_1$ just outside the yeast cell walls, implying that $j_{\text{cell}} = a_{\text{yeast}}c_1$. Our order-of-magnitude estimate of j_{cell} allows us then to estimate that $a_{\text{yeast}}c_1 \sim 2.5$ pg/(μm²h), which is in the

same order of magnitude as ac_1, the nutrient flux into the colony.

b. Consistency with nutrient screening length inside a yeast colony

In the main text, we use our measured value of ac_1, the mass flux into the colony, to calculate the nutrient screening length in the fluid $\ell = (\rho_0 \beta D)/a = 5 \pm 2$ mm. It is also possible to use the value of ac_1 to estimate the nutrient screening length *inside* the yeast colony given in [39]:

$$\zeta = \sqrt{\frac{D\rho_{\text{solute}}}{\dot{\rho}}}, \qquad (D3)$$

where $\rho_{\text{solute}} = \rho_0 \beta c_1$ is the characteristic density of solute, and $\dot{\rho}$ is the rate at which the solute is depleted. With the volume of a yeast cell $V_{\text{yeast}} = (4/3)\pi r_{\text{yeast}}^3$ and the packing fraction of spherical cells in a colony $\mathcal{N} \sim 0.5$, the value of $\dot{\rho}$ can then be estimated as

$$\dot{\rho} \sim \mathcal{N} \frac{j_{\text{col}} A_{\text{yeast}}}{V_{\text{yeast}}} = \frac{3\mathcal{N} ac_1}{r_{\text{yeast}}} \qquad (D4)$$

implying that the nutrient screening length inside the colony is

$$\zeta = \sqrt{\frac{D\rho_0 \beta r_{\text{yeast}}}{3\mathcal{N} a}} \sim 90 \ \mu\text{m}, \qquad (D5)$$

in approximate agreement with the work of Lavrentovich *et al.* [39].

APPENDIX E: NONDIMENSIONALIZING THE SET OF EQUATIONS

As we discuss in Sec. VI of the main text, after coupling the Navier-Stokes equations with the diffusing solute field, applying the Boussinesq approximation as the local density variations are small in our experiments ($\delta\rho/\rho_0 \ll 1$), and including the flux boundary condition below the yeast colony, we find

$$\frac{\partial c}{\partial t} + \mathbf{u} \cdot \nabla c = D\nabla^2 c, \qquad (E1)$$

$$\frac{\partial \mathbf{u}}{\partial t} + \mathbf{u} \cdot \nabla \mathbf{u} = -\frac{\nabla p}{\rho_0} + \nu\nabla^2 \mathbf{u} + \beta c\mathbf{g}, \qquad (E2)$$

$$\nabla \cdot \mathbf{u} = 0, \qquad (E3)$$

$$(\nabla c \cdot \hat{\mathbf{n}})|_{\text{colony}} = \left(\frac{c}{\ell}\right)\bigg|_{\text{colony}}, \qquad (E4)$$

where c is the nutrient concentration field, $\mathbf{u}$ the fluid velocity, D the nutrient diffusion constant in the substrate, ν the fluid's kinematic viscosity, ρ_0 the substrate density

without nutrient, p the fluid's pressure, $\mathbf{g} = -g\hat{\mathbf{z}}$ the downward acceleration due to gravity, β the solute expansion coefficient, $\hat{\mathbf{n}}$ the normal unit vector to the colony interface, and $\ell = \rho_0 \beta D/a$ the characteristic nutrient-depletion length in the substrate fluid.

To better understand the dynamics of our model, we nondimensionalize Eqs. (E1)–(E4) by choosing a characteristic length scale $L = H$, the height of the fluid in the Petri dish, a timescale $T = H^2/D$ (the time it takes solute to diffuse from the bottom to the top of the fluid in the Petri dish), and the initial *maximum* glucose concentration c_1 (the initial concentration has the maximum value before the yeast cells deplete nutrients). The nondimensionalized equations become

$$\frac{\partial \tilde{c}}{\partial \tilde{t}} + \tilde{\mathbf{u}} \cdot \nabla \tilde{c} = \nabla^2 \tilde{c}, \qquad (E5)$$

$$\frac{1}{\text{Sc}}\left[\frac{\partial \tilde{\mathbf{u}}}{\partial \tilde{t}} + \tilde{\mathbf{u}} \cdot \nabla \tilde{\mathbf{u}}\right] = -\nabla \tilde{p} + \nabla^2 \tilde{\mathbf{u}} - \text{Ra}\tilde{c}\,\hat{\mathbf{z}}, \quad (E6)$$

$$\nabla \cdot \tilde{\mathbf{u}} = 0, \qquad (E7)$$

where the dimensionless concentration field is given by $\tilde{c} = c/c_1$, the dimensionless velocity is $\tilde{u} = u/(L/T) = u/(D/H)$, and the dimensionless pressure is $\tilde{p} = p/(D\rho_0\nu/H^2)$. The nondimensional Navier-Stokes equation reveals two key dimensionless parameters: the Schmidt number $\text{Sc} = \nu/D$, the ratio of the momentum diffusion to solute diffusion, and the Rayleigh number $\text{Ra} = (H^3\beta c_1 g)/(D\nu)$, which quantifies the strength of the dimensionless buoyant force [37]. Nondimensionalizing the flux boundary condition for the concentration field at the yeast colony's border reveals a final key parameter; the boundary condition becomes

$$(\nabla \tilde{c} \cdot \hat{\mathbf{n}})|_{\text{colony}} = (G\tilde{c})|_{\text{colony}}, \qquad (E8)$$

where the "mass flux number" $G = (Ha)/(\rho_0\beta D) \equiv H/\ell$ is the dimensionless ratio of the fluid height H to the nutrient-depletion length in the fluid ℓ.

The interplay between the Rayleigh, Schmidt, and mass flux numbers in our simulated geometry controls the dynamics of our model. However, the large Schmidt number $\text{Sc} = \nu/D \sim 10^8$–$10^9$ (using the parameter values in Table II) allows us to set the inertial terms in Eq. (E6) to zero; this simplification corresponds to the Stokes regime. Thus, we need consider only the interplay between the Rayleigh and mass flux numbers. For the standard fluid height used in our experiments (40 mL of fluid in a standard 94-mm-diameter Petri dish, or $H = 7 \pm 0.2$ mm), the Rayleigh number ranges from 10^3 to 10^4 as we vary the fluid viscosity from $\eta = 54 \pm 8$ Pa s to $\eta = 600 \pm 90$ Pa s, and the mass flux number remains constant at $G \sim 4.4$. The yeast do not deplete nutrients quickly enough to allow us to

set $c = 0$ on the bottom of the colony, corresponding to the $G \to \infty$ limit. Both quantities consequently play a role in our experiments.

APPENDIX F: SIMULATION METHODS

In this appendix, we discuss how we utilize OPENFOAM 5.0 [40] to simulate the buoyant fluid flow created by our yeast colonies and the early stages of yeast colony growth. Specifically, we discuss the particular programs that we create, how we prepare meshes and geometries for use in OPENFOAM, and how we analyze and visualize simulation output.

1. `diffusionPressureFoam`

The program `diffusionPressureFoam` (available on GitHub [66]) simulates a yeast colony that absorbs a diffusing concentration field and calculates the resulting hydrostatic pressure. We use `diffusionPressureFoam` to show how the baroclinic instability begins before advection begins to dominate, as seen in Fig. 5.

To create `diffusionPressureFoam`, we modify the standard solver packaged with OPENFOAM called `laplacianFoam`, which simulates a diffusing scalar field. At each time step, we let the concentration field diffuse and possibly be absorbed by the yeast. We utilize SWAK4FOAM [67], an extension of OPENFOAM, to impose the absorption boundary condition that

$$(\nabla c \cdot \hat{n})|_{\text{colony}} = \left(\frac{ac}{\rho_0 \beta D}\right)\bigg|_{\text{colony}}. \tag{F1}$$

The hydrostatic pressure inside a fluid is given by [37]

$$\nabla p = \rho_0 (1 + \beta c)\mathbf{g}. \tag{F2}$$

However, to calculate the hydrostatic pressure numerically, we take the divergence of Eq. (F2) and solve

$$\nabla^2 p = \nabla \cdot [\rho_0 (1 + \beta c)\mathbf{g}]. \tag{F3}$$

At the free interface, we impose the boundary condition that $p = p_{\text{atmospheric}}$, while on other walls, we impose the condition (again using SWAK4FOAM [67]) that

$$[\nabla p \cdot \hat{n}]|_{\text{walls}} = [\rho_0 (1 + \beta c)\mathbf{g} \cdot \hat{n}]|_{\text{walls}}. \tag{F4}$$

We always assume radial symmetry when simulating yeast colonies on the surface of a viscous nutrient-containing liquid or at the bottom of a sealed Petri dish. To create our radially symmetric geometry, we use Gmsh 3.0.5 [68] to create a two-dimensional structured mesh spanning the Petri dish and then extrude it to form a wedge with an angle of 2.5° which is the appropriate setup for radially symmetric simulations in OPENFOAM. We
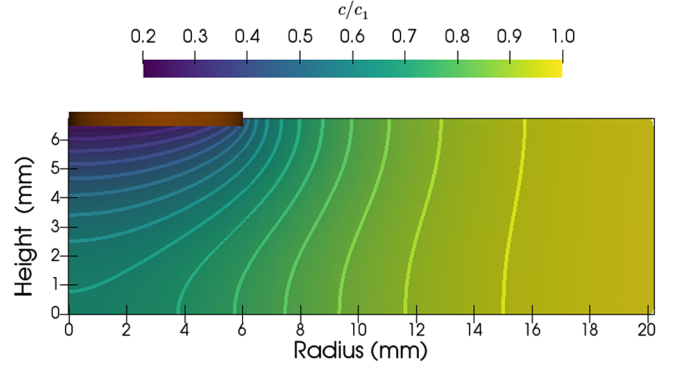
FIG. 16. Radially symmetric simulation of the concentration field c/c_1 below a yeast colony (the thick brown bar) on the surface of our viscous liquid after 48 h and at $\eta = 400 \pm 50$ Pa s. Equally spaced contours of constant concentration are shown.

simulate our experiments at a resolution such that 20 simulation cells span the yeast colony radius. We wrap the Gmsh geometry creation script in PYTHON scripts that can automatically generate geometries, change simulation parameters, and quickly analyze simulation output.

After running a simulation, we use PARAVIEW [69], an open-source tool to visualize large geometrical datasets, to visualize the results and create figures such as the concentration field shown in Fig. 16. To quickly analyze data from many simulations, we use automated PYTHON scripts to extract relevant data such as the velocity on the fluid's surface and the total amount of solute present in a Petri dish. To create the baroclinicity field $(1/\rho^2)(\nabla\rho \times \nabla p)$ seen in Fig. 5, we utilize the `funkySetFields` utility, a part of SWAK4FOAM [67], which can algebraically manipulate the output of OPENFOAM simulations.

2. `stokesBuoyantSoluteFoam`

The program `stokesBuoyantSoluteFoam` simulates how yeast depletes the density of the surrounding fluid and calculates the resulting fluid flow. We use this program to generate the quantitative agreement between experiment and simulation in Fig. 6. Specifically, `stokesBuoyantSoluteFoam` solves the dimensionless equations (E5)–(E7) and the dimensionless mass flux boundary condition below the yeast colony in Eq. (E8). It assumes that the Schmidt number $S_c = \nu/D$ is infinite (as we discuss above) and consequently solves

$$\frac{\partial \tilde{c}}{\partial \tilde{t}} + \tilde{\mathbf{u}} \cdot \nabla \tilde{c} = \nabla^2 \tilde{c}, \tag{F5}$$

$$0 = -\nabla \tilde{p} + \nabla^2 \tilde{\mathbf{u}} - \text{Ra}\tilde{c}\,\hat{\mathbf{z}}, \tag{F6}$$

$$\nabla \cdot \tilde{\mathbf{u}} = 0, \tag{F7}$$

$$(\nabla \tilde{c} \cdot \hat{\mathbf{n}})|_{\text{colony}} = (G\tilde{c})|_{\text{colony}} \tag{F8}$$

at each time step.

We again utilize SWAK4FOAM [67] to implement the concentration boundary condition at the yeast colony boundary [Eq. (F8)]. At each time step, the solute diffuses and is absorbed by the yeast. After diffusing, `stokes BuoyantSoluteFoam` calculates the steady-state velocity field using the same technique as `buoyant BoussinesqSimpleFoam` (the SIMPLE algorithm [70]) which is packaged with OPENFOAM. The velocity from the previous time step is used as an initial guess for the velocity field in the next time step to improve its convergence speed. To avoid stability problems resulting from a high Courant number [70], we adaptively change the time step to ensure that the maximum Courant number in the simulation remain below 0.5 and also use the implicit Crank-Nicolson technique [70] to evolve the concentration field. Geometry preparation and postprocessing for `stokesBuoyantSoluteFoam` is the same as that for `diffusionPressureFoam`.

3. `forcedThinFilmFoam`

`forcedThinFilmFoam` (available on GitHub [52]) solves Eq. (11) in the main text, or

$$\frac{\partial h(\mathbf{r}, t)}{\partial t} + \boldsymbol{\nabla} \cdot [h(\mathbf{r}, t)\mathbf{v}(\mathbf{r})]$$
$$= D_h \nabla^2 h(\mathbf{r}, t) + \mu h(\mathbf{r}, t)\left[1 - \frac{h(\mathbf{r}, t)}{h_0}\right], \quad \text{(F9)}$$

and leads to the radial height profiles shown in Fig. 9. Although we can simulate arbitrary velocity fields, we use the radially symmetric field of $\mathbf{v}(\mathbf{r}) = (1/2)\alpha r\hat{\mathbf{r}}$, matching Eq. (14).
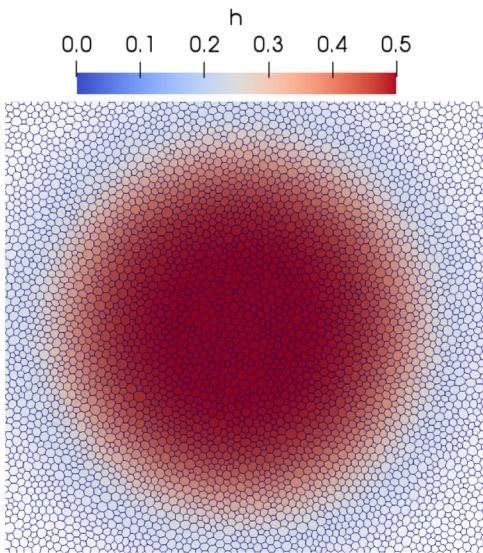
FIG. 17. A polyhedral dual mesh (blue cells) and corresponding height field h used by the `forcedThinFilmFoam` program [52].

We use `Gmsh 3.0.5` [68] to create a two-dimensional mesh in a circular domain mimicking a Petri dish as seen in Fig. 17. We find that the choice of mesh *dramatically* impacts simulation performance; using a regular Cartesian grid leads to pronounced lattice artifacts, likely because of the autocatalytic growth term on the right side of Eq. (F9). We obtain the best results when we convert a Delaunay triangular mesh to its dual polyhedral mesh using OPENFOAM's `polyDualMesh` utility, similar to other work simulating fluid flow in radial geometries [71].

To allow for advection-dominated simulations, we use a flux-limiting superbee scheme when calculating the divergence term, or $\boldsymbol{\nabla} \cdot [h(\mathbf{r}, t)\mathbf{v}(\mathbf{r})]$. To prevent stability problems, we ensure that the maximum Courant number is less than 0.1 and use the implicit Crank-Nicolson technique [70] to evolve the height field. We again utilize PYTHON scripts to analyze the data coupled with OPENFOAM's postprocessing `singleGraph` tool.

APPENDIX G: SIMULATED NUTRIENT ABSORPTION VS FLOW RATE

To investigate if microbial colonies generating buoyant flows absorb more nutrients than those that do not, we simulate a yeast colony on the surface of our fluid (again with a fixed colony radius for simplicity) and vary the substrate viscosity from 10 to 100 Pa s, allowing us to control the magnitude of the buoyant flow. We also simulate a substrate with infinite viscosity where no flow is allowed. We keep the rest of the simulation parameters fixed to the values in Table II with $H = 7$ mm and record
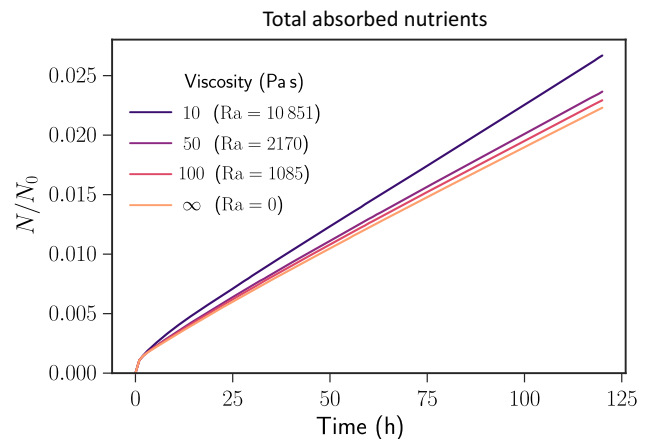
FIG. 18. Total number of nutrient molecules absorbed by the yeast relative to the original number of nutrient molecules in the fluid N/N_0 as the fluid viscosity is varied. The height of the fluid is $H = 7$ mm and the rest of the simulation parameters are set using the values in Table II. The Rayleigh number Ra $= (H^3\beta c_1 g)/(D\nu)$ varies from 0 to approximately 10^4 due to the changing viscosity ν, and the mass flux number $G = (Ha)/(\rho_0\beta D) \equiv H/\ell$ is fixed at $G \approx 4.4$. Note that the stronger advection of the substrate fluid at lower viscosities leads to an enhanced uptake of nutrient molecules.

the nutrient uptake by the colony over time. The Rayleigh number Ra $= (H^3 \beta c_1 g)/(D\nu)$ of these simulations ranges between 0 and 10^4, and the mass flux number $G = (Ha)/(\rho_0 \beta D) \equiv H/\ell$ is fixed at $G \approx 4.4$. As shown in Fig. 18, the more vigorous flows associated with smaller substrate viscosities allow yeast colonies to absorb nutrients more efficiently; the nutrient absorption rate at 10 Pa s is about 1.5 times larger than at infinite viscosity. It is possible that microbes growing on less viscous fluids can induce more intense flows, enhancing this effect even further. It thus seems plausible that colonies generating stronger buoyant flows can indeed have a selective advantage.

---

[1] T. Tél, A. de Moura, C. Grebogi, and G. Károlyi, *Chemical and Biological Activity in Open Flows: A Dynamical System Approach*, Phys. Rep. **413**, 91 (2005).

[2] E. R. Abraham, *The Generation of Plankton Patchiness by Turbulent Stirring*, Nature (London) **391**, 577 (1998).

[3] E. R. Abraham, C. S. Law, P. W. Boyd, S. J. Lavender, M. T. Maldonado, and A. R. Bowie, *Importance of Stirring in the Development of an Iron-Fertilized Phytoplankton Bloom*, Nature (London) **407**, 727 (2000).

[4] F. D'Ovidio, S. De Monte, S. Alvain, Y. Dandonneau, and M. Levy, *Fluid Dynamical Niches of Phytoplankton Types*, Proc. Natl. Acad. Sci. U.S.A. **107**, 18366 (2010).

[5] Z. I. Johnson, *Niche Partitioning among Prochlorococcus Ecotypes along Ocean-Scale Environmental Gradients*, Science **311**, 1737 (2006).

[6] M. J. Follows, S. Dutkiewicz, S. Grant, and S. W. Chisholm, *Emergent Biogeography of Microbial Communities in a Model Ocean*, Science **315**, 1843 (2007).

[7] O. Hallatschek, P. Hersen, S. Ramanathan, and D. R. Nelson, *Genetic Drift at Expanding Frontiers Promotes Gene Segregation*, Proc. Natl. Acad. Sci. U.S.A. **104**, 19926 (2007).

[8] K. S. Korolev, M. Avlund, O. Hallatschek, and D. R. Nelson, *Genetic Demixing and Evolution in Linear Stepping Stone Models*, Rev. Mod. Phys. **82**, 1691 (2010).

[9] K. S. Korolev, M. J. I. Müller, N. Karahan, A. W. Murray, O. Hallatschek, and D. R. Nelson, *Selective Sweeps in Growing Microbial Colonies*, Phys. Biol. **9**, 026008 (2012).

[10] M. Gralka, F. Stiewe, F. Farrell, W. Möbius, B. Waclaw, and O. Hallatschek, *Allele Surfing Promotes Microbial Adaptation from Standing Variation*, Ecol. Lett. **19**, 889 (2016).

[11] B. T. Weinstein, M. O. Lavrentovich, W. Möbius, A. W. Murray, and D. R. Nelson, *Genetic Drift and Selection in Many-Allele Range Expansions*, PLoS Comput. Biol. **13**, e1005866 (2017).

[12] M. J. I. Muller, B. I. Neugeboren, D. R. Nelson, and A. W. Murray, *Genetic Drift Opposes Mutualism during Spatial Population Expansion*, Proc. Natl. Acad. Sci. U.S.A. **111**, 1037 (2014).

[13] M. F. Weber, G. Poxleitner, E. Hebisch, . Frey, and M. Opitz, *Chemical Warfare and Survival Strategies in Bacterial Range Expansions*, J. R. Soc. Interface **11**, 20140172 (2014).

[14] L. McNally, E. Bernardy, J. Thomas, A. Kalziqi, J. Pentz, S. P. Brown, B. K. Hammer, P. J. Yunker, and W. C. Ratcliff, *Killing by Type VI Secretion Drives Genetic Phase Separation and Correlates with Increased Cooperation*, Nat. Commun. **8**, 14371 (2017).

[15] M. O. Lavrentovich, M. E. Wahl, D. R. Nelson, and A. W. Murray, *Spatially Constrained Growth Enhances Conversional Meltdown*, Biophys. J. **110**, 2800 (2016).

[16] S. Pigolotti, R. Benzi, P. Perlekar, M. H. Jensen, F. Toschi, and D. R. Nelson, *Growth, Competition and Cooperation in Spatial Population Genetics*, Theor. Popul. Biol. **84C**, 72 (2013).

[17] S. Pigolotti, R. Benzi, M. H. Jensen, and D. R. Nelson, *Population Genetics in Compressible Flows*, Phys. Rev. Lett. **108**, 128102 (2012).

[18] P. Perlekar, R. Benzi, D. R. Nelson, and F. Toschi, *Population Dynamics at High Reynolds Number*, Phys. Rev. Lett. **105**, 144501 (2010).

[19] T. Chotibut, D. R. Nelson, and S. Succi, *Striated Populations in Disordered Environments with Advection*, Physica (Amsterdam) **465A**, 500 (2017).

[20] B. T. Weinstein, *Microbial Evolutionary Dynamics and Transport on Solid and Liquid Substrates*, Ph.D. thesis, Harvard University, 2018.

[21] M. B. Short, C. A. Solari, S. Ganguly, T. R. Powers, J. O. Kessler, and R. E. Goldstein, *Flows Driven by Flagella of Multicellular Organisms Enhance Long-Range Molecular Transport*, Proc. Natl. Acad. Sci. U.S.A. **103**, 8315 (2006).

[22] A. J. T. M. Mathijssen, F. Guzmán-Lastra, A. Kaiser, and H. Löwen, *Nutrient Transport Driven by Microbial Active Carpets*, Phys. Rev. Lett. **121**, 248101 (2018).

[23] L. Vaccari, M. Molaei, T. H. R. Niepa, D. Lee, R. L. Leheny, and K. J. Stebe, *Films of Bacteria at Interfaces*, Adv. Colloid Interface Sci. **247**, 561 (2017).

[24] D. Boutelier, A. Cruden, and B. Saumur, *Density and Visco-Elasticity of Natrosol 250 HH Solutions: Determining Their Suitability for Experimental Tectonics*, J. Struct. Geol. **86**, 153 (2016).

[25] D. Vella and L. Mahadevan, *The Cheerios Effect*, Am. J. Phys. **73**, 817 (2005).

[26] J. S. Langer, *Theory of Spinodal Decomposition in Alloys*, Ann. Phys. (N.Y.) **65**, 53 (1971).

[27] L. Rayleigh, *On the Instability of Jets*, Proc. London Math. Soc. **1**, 4 (1878).

[28] J. Eggers, *Nonlinear Dynamics and Breakup of Free-Surface Flows*, Rev. Mod. Phys. **69**, 865 (1997).

[29] L. E. Scriven and C. V. Sternling, *The Marangoni Effects*, Nature (London) **187**, 186 (1960).

[30] T. E. Angelini, M. Roper, R. Kolter, D. A. Weitz, and M. P. Brenner, *Bacillus Subtilis Spreads by Surfing on Waves of Surfactant*, Proc. Natl. Acad. Sci. U.S.A. **106**, 18109 (2009).

[31] A. Yang, W. S. Tang, T. Si, and J. X. Tang, *Influence of Physical Effects on the Swarming Motility of Pseudomonas Aeruginosa*, Biophys. J. **112**, 1462 (2017).

[32] D. B. Kearns, *A Field Guide to Bacterial Swarming Motility*, Nat. Rev. Microbiol. **8**, 634 (2010).

[33] S. Soh, K. J. M. Bishop, and B. A. Grzybowski, *Dynamic Self-Assembly in Ensembles of Camphor Boats*, J. Phys. Chem. B **112**, 10848 (2008).

[34] J. S. Turner, *Buoyancy Effects in Fluids*, 1st ed. (Cambridge University Press, Cambridge, England, 1973).

[35] M. R. Benoit, R. B. Brown, P. Todd, E. S. Nelson, and D. M. Klaus, *Buoyant Plumes from Solute Gradients Generated by Non-Motile E. coli*, Phys. Biol. **5,** 046007 (2008).

[36] D. H. Sharp, *An Overview of Rayleigh-Taylor Instability*, Physica (Amsterdam) **12D,** 3 (1984).

[37] E. Guyon, J.-P. Hulin, L. Petit, and C. D. Mitescu, *Physical Hydrodynamics*, 2nd ed. (Oxford University Press, New York, 2015).

[38] J. Marshall and A. R. Plumb, *Atmosphere, Ocean, and Climate Dynamics*, 1st ed. (Academic Press, Boston, 2008).

[39] M. O. Lavrentovich, J. H. Koschwanez, and D. R. Nelson, *Nutrient Shielding in Clusters of Cells*, Phys. Rev. E **87,** 062703 (2013).

[40] H. G. Weller, G. Tabor, H. Jasak, and C. Fureby, *A Tensorial Approach to Computational Continuum Mechanics Using Object-Oriented Techniques*, Comput. Phys. **12,** 620 (1998).

[41] B. T. Weinstein, stokesBuoyantSoluteFoam, GitHub, 2018.

[42] G. K. Batchelor, *An Introduction to Fluid Dynamics* (Cambridge University Press, Cambridge, England, 2000).

[43] F. Melo, J. F. Joanny, and S. Fauve, *Fingering Instability of Spinning Drops*, Phys. Rev. Lett. **63,** 1958 (1989).

[44] J.-i. Wakita, K. Komatsu, A. Nakahara, T. Matsuyama, and M. Matsushita, *Experimental Investigation on the Validity of Population Dynamics Approach to Bacterial Colony Formation*, J. Phys. Soc. Jpn. **63,** 1205 (1994).

[45] J. D. Murray, *Mathematical Biology II: Spatial Models and Biomedical Applications*, 3rd ed. (Springer, New York, 2011).

[46] D. J. Bergman, *Third Sound in Superfluid Helium Films of Arbitrary Thickness*, Phys. Rev. A **3,** 2058 (1971).

[47] I. Klapper and J. Dockery, *Finger Formation in Biofilm Layers*, SIAM J. Appl. Math. **62,** 853 (2002).

[48] D. A. Head, *Linear Surface Roughness Growth and Flow Smoothening in a Three-Dimensional Biofilm Model*, Phys. Rev. E **88,** 032702 (2013).

[49] F. D. C. Farrell, O. Hallatschek, D. Marenduzzo, and B. Waclaw, *Mechanically Driven Growth of Quasi-Two-Dimensional Microbial Colonies*, Phys. Rev. Lett. **111,** 168101 (2013).

[50] A. Giometto, D. R. Nelson, and A. W. Murray, *Physical Interactions Reduce the Power of Natural Selection in Growing Yeast Colonies*, Proc. Natl. Acad. Sci. U.S.A. **115,** 11448 (2018).

[51] H. A. Stone and A. Ajdari, *Hydrodynamics of Particles Embedded in a Flat Surfactant Layer Overlying a Subphase of Finite Depth*, J. Fluid Mech. **369,** 151 (1998).

[52] B. T. Weinstein, forcedThinFilmFoam, GitHub, 2018.

[53] I. Steinbach, *Pattern Formation in Constrained Dendritic Growth with Solutal Buoyancy*, Acta Mater. **57,** 2640 (2009).

[54] L. Keiser, H. Bense, P. Colinet, J. Bico, and E. Reyssat, *Marangoni Bursting: Evaporation-Induced Emulsification of Binary Mixtures on a Liquid Layer*, Phys. Rev. Lett. **118,** 074504 (2017).

[55] L. W. Schwartz, *Viscous Flows Down an Inclined Plane: Instability and Finger Formation*, Physics Fluids A **1,** 443 (1989).

[56] S. R. Waitukaitis, H. F. Grütjen, J. R. Royer, and H. M. Jaeger, *Droplet and Cluster Formation in Freely Falling Granular Streams*, Phys. Rev. E **83,** 051302 (2011).

[57] L. D. Li, T. Crouzier, A. Sarkar, L. Dunphy, J. Han, and K. Ribbeck, *Spatial Configuration and Composition of Charge Modulates Transport into a Mucin Hydrogel Barrier*, Biophys. J. **105,** 1357 (2013).

[58] F. Tesser, J. C. H. Zeegers, H. J. H. Clercx, L. Brunsveld, and F. Toschi, *Finite-Size Effects on Bacterial Population Expansion under Controlled Flow Conditions*, Sci. Rep. **7,** 43903 (2017).

[59] R. B. Bird, R. C. Armstrong, and O. Hassager, *Dynamics of Polymeric Liquids*, 2nd ed. (John Wiley & Sons, Inc., New York, 1987).

[60] W. Ostwald, *Ueber die Geschwindigkeitsfunktion der Viskosität Disperser Systeme. I*, Kolloid Z. **36,** 99 (1925).

[61] A. de Waele, *Viscometry and Plastometry*, Oil Color Chem. Assoc. J. **6,** 33 (1923).

[62] J. Rumble, *CRC Handbook of Chemistry and Physics*, 98th ed. (CRC Press, Boca Raton, 2017).

[63] L. Debnath and D. Bhatta, *Integral Transforms and Their Applications*, 1st ed. (CRC Press, Boca Raton, 2016).

[64] C. Culbertson, S. C. Jacobson, and J. M. Ramsey, *Diffusion Coefficient Measurements in Microfluidic Devices*, Talanta **56,** 365 (2002).

[65] J. L. DeRisi, V. R. Iyer, and P. O. Brown, *Exploring the Metabolic and Genetic Control of Gene Expression on a Genomic Scale*, Science **278,** 680 (1997).

[66] B. T. Weinstein, diffusionPressureFoam, GitHub, 2018.

[67] B. F. W. Gschaider, Swiss Army Knife for Foam, GitHub, 2018, https://github.com/Unofficial-Extend-Project-Mirror/openfoam-extend-swak4Foam-dev/.

[68] C. Geuzaine and J.-F. Remacle, Gmsh: *A 3-D Finite Element Mesh Generator with Built-In Pre- and Post-Processing Facilities*, Int. J. Numer. Methods Eng. **79,** 1309 (2009).

[69] U. Ayachit, *The ParaView Guide: A Parallel Visualization Application* (Kitware Inc., 2015).

[70] J. H. Ferziger and M. Perić, *Computational Methods for Fluid Dynamics* (Springer, Berlin, 2002).

[71] P. Vita, B. F. W. Gschaider, D. Prieling, and H. Steiner, *Thin Film Flow Simulation on a Rotating Disc*, in *Proceedings of the European Congress on Computational Methods in Applied Sciences and Engineering (ECCOMAS)*, 2012.

[72] See Supplemental Material at http://link.aps.org/supplemental/10.1103/PhysRevX.9.021058 for corresponding videos and their description.